Journal Pre-proofs

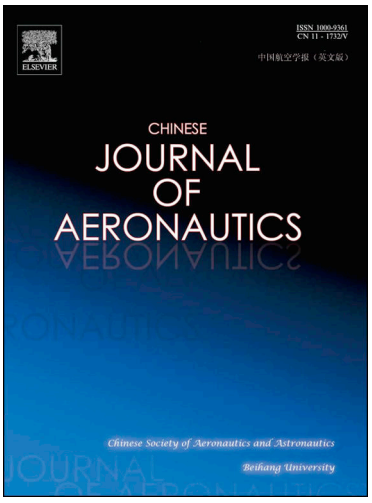

Full Length Article

Automatic interval management for aircraft based on dynamic fuzzy speed control considering uncertainty

Jie Yuan, Yang Pei, Yan Xu, Xiaochen Li, Yuxue Ge

PII: S1000-9361(23)00238-8
DOI: https://doi.org/10.1016/j.cja.2023.07.008
Reference: CJA 2721

To appear in: *Chinese Journal of Aeronautics*

Received Date: 2 November 2022
Revised Date: 2 April 2023
Accepted Date: 16 May 2023

Please cite this article as: J. Yuan, Y. Pei, Y. Xu, X. Li, Y. Ge, Automatic interval management for aircraft based on dynamic fuzzy speed control considering uncertainty, *Chinese Journal of Aeronautics* (2023), doi: https://doi.org/10.1016/j.cja.2023.07.008

Contents lists available at ScienceDirect

Chinese Journal of Aeronautics

Journal homepage: www.elsevier.com/locate/cja

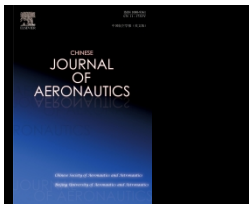

Automatic interval management for aircraft based on dynamic fuzzy speed control considering uncertainty

Jie YUAN[a,b], Yang PEI[a], Yan XU [b], Xiaochen LI[a], Yuxue GE[a,*]

[a]*School of Aeronautics, Northwestern Polytechnical University, Shaanxi 710072, China*

[b]*School of Aerospace, Transport and Manufacturing, Cranfield University, MK43 0AL, United Kingdom*

Received 2 November 2022; revised 2 April 2023; accepted 16 May 2023

Abstract

A novel real-time autonomous Interval Management System (IMS) is proposed to automate interval management, which considers the effect of wind uncertainty using the Dynamic Fuzzy Velocity Decision (DFVD) algorithm. The membership function can be generated dynamically based on the True Air Speed (TAS) limitation changes in real time and the interval criterion of the adjacent aircraft, and combined with human cognition to formulate fuzzy rules for speed adjusting decision-making. Three groups of experiments were conducted during the en-route descent stage to validate the proposed IMS and DFVD performances, and to analyze the impact factors of the algorithm. The verification experimental results show that compared with actual flight status data under controllers' command, the IMS reduces the descent time by approaching 30% with favorable wind uncertainty suppression performance. Sensitivity analysis shows that the ability improvement of DFVD is mainly affected by the boundary value of the membership function. Additionally, the dynamic generation of the velocity membership function has greater advantages than the static method in terms of safety and stability. Through the analysis of influencing factors, we found that the interval criterion and aircraft category have no significant effect on the capability of IMS. In a higher initial altitude scenario, the initial interval should be appropriately increased to enhance safety and efficiency during the descent process. This prototype system could evolve into a real-time Flight-deck Interval Management (FIM) tool in the future.

Keywords: Air transportation; Air traffic control; Safety interval; Fuzzy logic; Wind uncertainty

* Corresponding author. *E-mail address:* yuxuege@gmail.com

1. Introduction

The prediction disclosed by International Air Transportation Association shows that air passenger numbers rose from 3.326 billion to 4.54 billion between 2014 and 2019.[1] While the COVID-19 pandemic has had an impact on air travel, it is predicted that air traffic will recover by 2024.[2] There will be a predictable and substantial increase in passengers and air traffic volumes in the future.[3] The growing demand requires synchronous improvements in infrastructure, airspace structure, operation strategy, and more.

From an Air Traffic Management (ATM) perspective, tactical decisions made by air traffic controllers have barely changed in en-route operations over the past 50 years.[4] Controllers are likely to be affected by abilities and habits when commanding aircraft. And they also experience a "critical" or even "overloaded" working state for long periods with the dense traffic flow in busy airspace.[5] Therefore, ATM needs to be reformed to support future Trajectory Based Operations (TBO).

Aircraft automatic Interval Management (IM) is a significant strategy to support TBO. The National Aeronautics and Space Administration (NASA) believes that future air traffic systems will be replaced by a distributed collaborative ATM system and proposes the concept of an aircraft autonomous IM.[6] EUROCONTROL regards airborne interval management as an essential operational change to trigger structural alterations for European ATM.[7] The Civil Aviation Administration of China (CAAC) proposes a multi-mode interval management operation. The conflict detection and interval assurance tasks originally undertaken by Air Traffic Controllers (ATC) will be partially or fully delegated to the airborne equipment under the conditions of airspace, traffic flow, and proper air-ground coordination.[8] Through IM, air traffic efficiency and runway throughput can be improved,[9] fuel consumption for arriving traffic can be reduced in continuous descent operation mode,[10] the safe sequencing of aircraft on different routes when passing through intersections can be realized,[11] the predictability of aircraft trajectory can be increased,[12] etc.

Fortunately, the development of technologies such as Automatic Dependent Surveillance-Broadcast (ADS-B) in/out and satellite positioning have made it possible for the Flight Management System (FMS) to undertake some of the ATM work.[13] In addition, the advancement of airborne meteorological equipment enables providing accurate meteorological data for aircraft.[14] This progress makes it possible for the FMS to implement automatic IM based on the current operating environment. However, there are still many uncertainties during flight, among which the position deviation caused by uncertain wind is a significant component.[15]

The essence of autonomous IM is to achieve airborne Flight-deck Interval Management (FIM) by adjusting the flight speed and path.[16,17] By modifying the existing NASA spacing algorithm, Swieringa et al.[18] improved the performance of the following aircraft under delay. Waypoint selection methods can also realize autonomous IM by adjusting the horizontal trajectory.[19,20] However, studies have shown that adjustment based on flight speed is a better solution.[21] Tang and Zheng[22] proposed a hybrid IM strategy by integrating the following theory with the speed adjustment strategy based on the rolling time domain, which improved the maneuvering efficiency under IM. Hubbs and Shay[23] improved the performance of the IM avionics prototype based on aircraft performance, which reduced the workload of pilots. The Brittain team conducted a series of research on route safety IM based on the reinforcement learning algorithm. Research on route and speed decision-making for controllers for a pair of aircraft is discussed in Refs. 24, 25. Subsequent research treated aircraft as agents and realized the autonomous decision-making of multiple aircraft during the route operation phase.[26] Control algorithms can also address IM problems. Based on the Markov decision method, Gaydos implemented IM by solving the control rate.[27] Weitz and Swieringa[28] compared the characteristics of two-speed control laws that implement IM functions. But these do not consider the performance differences of different aircraft and do not address terminal operation.

As a significant area for aircraft distribution, the terminal area has the characteristics of dense traffic flow and numerous conflict points[29], which increases the workload of controllers. Therefore, the trade-off between safety and efficiency becomes more pronounced in terminal areas. Brittain and Wei[30] suggested that the proposed method can be applied to terminal airspace, but it has not been tested. Riedel et al.[31] used the particle swarm algorithm with speed constraints to achieve a balance between IM and fuel saving in the descent phase. Barmore et al.[32] used proportional control and ground speed feedback to compute the speed compensation required to eliminate the spacing errors and employed a human-in-loop approach to achieve delay absorption during descent in the terminal IM.

When manually judging the distance and speed between a pair of adjacent aircraft, there are often no clear boundaries. These unclear features make controllers have the ability to solve or make decisions of complex, nonlinear, and incompletely known rules such as IM instead of machines. The fuzzy decision-making provides a feasible solution for IM. Fuzzy logic can handle the concept of partial truth values between "completely true" and "completely false".[33] A fuzzy model can be built up directly through ATC expertise which can be expressed by a set of heuristic rules quantified according to fuzzy set theory.[34]

When using fuzzy logic for decision-making, traditional research typically involves fixing the parameters of the membership function and using consistent functions for the entire decision-making process. This method has been successfully applied in various applications, such as drone collision avoidance[35], quality assessment of 4-Dimensional Trajectory (4DT)[36], control of ground traffic lights[37], and aircraft clearance decision-making[38]. While static membership functions can handle simple decision-making problems, more complex problems require a more fine-grained approach by increasing the division of the universe of discourse and adding fuzzy rules. For instance, Ören and Yücel[39] used 487 rules to model landing sequences, and Volpe Lovato et al.[40] used two fuzzy models with 171 rules to remove conflicts during the en-route flight phase. Actually, in real-world scenarios, the variation range of decision variables may change in real time, which requires more flexible decision-making. If static membership functions are used in this complex scenario, more factors need to be considered, resulting in more detailed divisions and rules for making high-quality decision. This may raise parameters adjusting challenges and require complex experiments to explore the operation laws. To address this issue, we propose a novel method of dynamically generating membership functions to simplify the complexity of fine division of the universe of discourse, numerous rules, and difficult parameter adjustment in the design process of static fuzzy decision-making methods. This method specifically addresses the complexity of the flight en-route descent phase, which is a critical area in decision-making.

In the light of the above discussion, previous research on IM focused on a simplified two-aircraft model consisting of a front and rear aircraft during the en-route phase, as shown in the dotted box in Fig. 1. Compared with the route operations, the descent stage in the terminal area has a more complex operating environment and uncertainties, which brings more challenges to achieve IM. Moreover, the performance differences among various aircraft types further complicate interval management during the descent. It is difficult to use accurate numerical values to characterize the motion state and interval distance between aircraft sequences in this complex scenario, which is a significant reason for simplifying the problem in the previous study. The bottom left corner of Fig. 1 shows significant factors that were rarely comprehensively considered in previous studies. To deal with the above difficulties, this paper proposes a dynamic speed control prototype system based on fuzzy logic theory, as shown by the right solid line box in Fig. 1. This approach overcomes the limitations of traditional static fuzzy decision-making by dynamically adjusting the descending flight speed according to the flight performance of multi-aircraft in real time to ensure the minimum interval. The prototype system can also adapt to uncertain conditions.

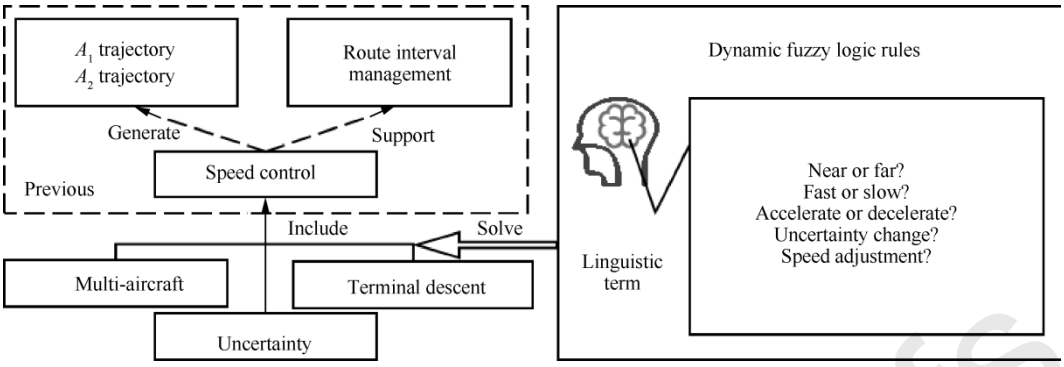

Fig. 1 Highlights of this paper.

Subsequent sections are organized as follows. Section 2 describes the research problem and builds the fundamental model required for the IM problem. Section 3 shows the operation flow of the Interval Management System (IMS) prototype based on Dynamic Fuzzy Velocity Decision (DFVD) algorithm, and introduces its design method in detail for the key steps. Section 4 conducts validity verification, sensitivity analysis, and impact factor analysis experiments of the proposed method based on formulating evaluation indicators and experimental scenarios. At the same time, we analyze the experimental results.

2. Computation scheme

It is significant to ensure the safety of multi-aircraft intervals and reduce spacing to improve operational efficiency, especially in terminal area. Uncertainty increases the difficulty of aircraft interval management. In this section, we construct the 4DT model, formulate an uncertainty model during flight, and analyze safety and flight constraints.

2.1. Problem formulation

Safe interval between aircraft is required at all flight phases, while the characteristics of sequence, high volume of traffic, and potential for conflicts make the en-route descent phase be a significant process to realize IM. The research object is to realize the automatic IM for aircraft sequence in the terminal area with uncertainty by adjusting the aircraft speed. We made several assumptions and explanations to make the study feasible.

Specifically, we assume that aircraft can receive the flight speed and position coordinates from the ADS-B data of the front and the rear aircraft, and the data are unbiased. The flight parameter simulator aboard is constructed based on the user manual for the Base of Aircraft Data (BADA) with Indicated Air Speed (IAS) flight mode. The flights in the research are not affected by factors other than uncertainty wind, and the wind model is known. The research phase starts at the point about to descend on the route and ends before the final approach. The phase is preceded by the Standard Terminal Arrival Route (STAR), and it starts at point S on the route and ends at point F, where the aircraft descends to an altitude of about 2000 m above the ground as shown in Figs. 2 and 3. We consider a group of target aircraft flying within 90° clockwise and counterclockwise in the approach direction of the runway, and assume that their order is fixed and cannot be changed as they intercept a public route segment R_p.

2.2. 4DT en-route descent model

The positions of the original aircraft ($A_{\mathrm{o},i}$, i = 1, …, i–1, i, i+1, …, N_{A}) transform to a same reference datum at first as shown in Fig. 2. $A_{\mathrm{o},i}$ and $A_{\mathrm{o},i+1}$ are flying at FL256 (Flight Level 256), and $A_{\mathrm{o},1}$ and $A_{\mathrm{o},i-1}$ are respectively flying at FL236 and FL276. Taking FL256 as the datum plane, $A_{\mathrm{o},1}$ and $A_{\mathrm{o},i-1}$ are projected to the plane and denoted as $A^{\mathrm{p}}_{\mathrm{o},1}$ and $A^{\mathrm{p}}_{\mathrm{o},i-1}$. Then straighten the flight route and arrange aircraft on the same straight line according to the remaining flight distance. $A_{\mathrm{o},i}$ is recorded as A_i after position conversion.

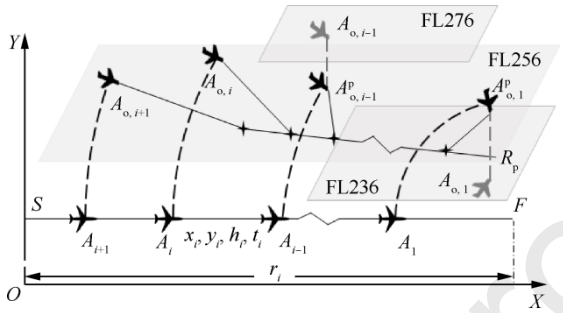

Fig. 2 Horizontal profiles and their conversion method of multi-aircraft during approach.

The conversed real-time 4DT of A_i is denoted as x_i, y_i, h_i, and t_i, and specifically, these are on-track distance, off-track distance (a constant value in the research), flight altitude, and elapsed flight time. Denote A_i as the current aircraft, and A_{i-1} and A_{i+1} are the front and rear aircraft, respectively. The intervals between A_i and them are $d_{i-1,i}$ and $d_{i,i+1}$, which must be longer than the specified interval criterion at any time during the flight. Conversed vertical profiles of multi-aircraft in the same en-route procedure are shown in Fig. 3.

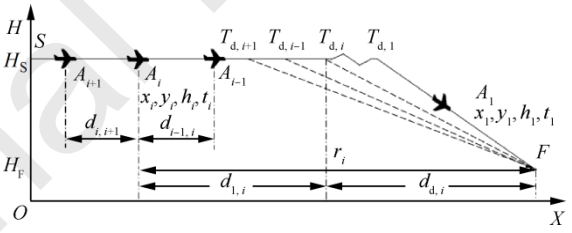

Fig. 3 Conversed vertical profiles of multi-aircraft during approach.

H_S, H_F, and $T_{\mathrm{d},i}$ represent the start altitude, the final altitude, and the Top of Descent (TOD) point for A_i, respectively. r_i, $d_{\mathrm{l},i}$, $d_{\mathrm{d},i}$ are en-route descent range, level flight distance, and descent distance of A_i, respectively, satisfying $r_i = d_{\mathrm{l},i} + d_{\mathrm{d},i}$. Denote the IAS of A_i as $V_{\mathrm{I},i}$. Taking Δt as the time unit, the 4DT of A_i can be defined mathematically by the following equation:

$$\begin{cases} t_{i,j}(\Delta t) = t_{i,j-1} + \Delta t \\ x_{i,j}(\Delta t) = x_{i,j-1} + V_{\mathrm{T},i,j}\Delta t \\ y_{i,j}(\Delta t) = y_{i,j-1} = \text{constant} \\ h_{i,j}(\Delta t) = \begin{cases} H_S & x_{i,j} \le d_{\mathrm{l},i} \\ h_{i,j-1} - r_{\mathrm{d},i,j}\Delta t & x_{i,j} > d_{\mathrm{l},i} \end{cases} \end{cases} \tag{1}$$

where the subscript j is the count of Δt, that is the jth time unit. $V_{\mathrm{T},i,j}$ is the True Air Speed (TAS). $r_{\mathrm{d},i,j}$ is the descent rate, which can be generally calculated as

$$r_{\mathrm{d}} = \frac{(D-T)V_{\mathrm{T}}}{m_{\mathrm{A}}g} f\{Ma\} \tag{2}$$

where D, T, m_{A}, g, and Ma are the drag, thrust, mass, gravitational acceleration, and Mach number of the aircraft, respectively, which are continuously changing in real time.

The energy sharing factor $f\{Ma\}$ is only the function of current Ma and obtained by BADA.[41] V_{T} and Ma are derived from a given V_{I} as

$$\begin{cases} V_{\mathrm{T}} = Ma \cdot a \\ Ma = \sqrt{\dfrac{2}{K'}\left\{\left[\left(1+\dfrac{K'}{2}\left(\dfrac{V_{\mathrm{I}}}{a_0}\right)^2\right)^{\frac{K}{K'}}-1\right]\Big/\left(\dfrac{p}{p_0}\right)+1\right\}^{\frac{K'}{K}}-1} \end{cases} \tag{3}$$

where a and a_0 are the speed of sound in non-standard and standard atmosphere at flight height and sea level, respectively. K=1.4 is the isentropic expansion coefficient for air, $K' = K - 1 = 0.4$; p and p_0 are the non-standard and standard atmospheric pressure at flight height and sea level, respectively.

Supposing that aircraft descend with the reference IAS ($V_{\mathrm{I,r},i,j}$), $d_{\mathrm{l},i}$ and $d_{\mathrm{d},i}$ can be derived in reverse as follows:

$$d_{\mathrm{l},i} = r_i - d_{\mathrm{d},i} = r_i - \sum_{j=1}^{h_{i,j}=H_S} V_{\mathrm{T},i,j}(V_{\mathrm{I,r},i,j}) \times \Delta t \tag{4}$$

2.3. Uncertainty modeling

The uncertainty during the flight greatly affects the aircraft's judgment of the current condition and future separation trends. There are many uncertain factors during the flight, such as wind uncertainty and measurement error. Wind uncertainty is a significant factor affecting 4DT[42], and its uncertainty is mainly due to the random noise wind. Denote $V_{\mathrm{u}}(t)$ as the speed uncertainty caused by wind[43], which consists of gust $V_{\mathrm{u,g}}(t)$, gradual change wind $V_{\mathrm{u,c}}(t)$, and random noise wind $V_{\mathrm{u,n}}(t)$, with details in Eq.(5).

$$V_{\mathrm{u}}(t) = V_{\mathrm{u,g}}(t) + V_{\mathrm{u,c}}(t) + V_{\mathrm{u,n}}(t) \tag{5}$$

Gust can describe the sudden change of wind, which can be calculated as follows:

$$V_{\mathrm{u,g}}(t)=\begin{cases}V_{\mathrm{u,g,max}}\left[1-\cos 2\pi\left(\dfrac{t-t_{\mathrm{g1}}}{t_{\mathrm{g}}}\right)\right] & t_{\mathrm{g1}}<t<t_{\mathrm{g1}}+t_{\mathrm{g}}\\ 0 & \text{others}\end{cases} \tag{6}$$

where $V_{\mathrm{u,g,max}}$ is the maximum speed of gust; t_{g1} and t_{g} are the starting and duration time of the gust, respectively.

Gradual change wind represents the gradual change character of wind speed, as shown in:

$$V_{\mathrm{u,c}}(t)=\begin{cases}V_{\mathrm{u,c,max}}\left(\dfrac{t-t_{\mathrm{c1}}}{t_{\mathrm{c2}}-t_{\mathrm{c1}}}\right) & t_{\mathrm{c1}}<t\le t_{\mathrm{c2}}\\ V_{\mathrm{u,c,max}} & t_{\mathrm{c2}}<t\le t_{\mathrm{c2}}+t_{\mathrm{c}}\\ 0 & \text{others}\end{cases} \tag{7}$$

where $V_{\mathrm{u,c,max}}$, t_{c1}, t_{c2}, t_{c} represent the peak speed, starting time, ending time, and duration of gradual change wind, respectively.

Random noise wind can reflect the turbulence during the whole process, which can be characterized by a power spectral density that is denoted as $P\left(\omega_{i_{\mathrm{n}}}\right)$:

$$V_{\mathrm{u,n}}(t)=2\sum_{i_{\mathrm{n}}=1}^{N_{\mathrm{n}}}\left[P\left(\omega_{i_{\mathrm{n}}}\right)\Delta\omega\right]^{\frac{1}{2}}\cos\left(\omega_{i_{\mathrm{n}}}t+\varphi_{i_{\mathrm{n}}}\right) \tag{8}$$

where N_{n} is the points count of the upper cut-off frequency; $\Delta\omega$ indicates the frequency step, $\omega_{i_{\mathrm{n}}}=\left(i_n-1/2\right)\Delta\omega$; $\varphi_{i_{\mathrm{n}}}$ is a random variable uniformly distributed over the interval [0, 2π].

The calculation method of $P\left(\omega_{i_{\mathrm{n}}}\right)$ is shown as follows:

$$P\left(\omega_{i_{\mathrm{n}}}\right)=\frac{\mathrm{I}^2 l\overline{V_{\mathrm{n}}}}{\left(1+1.5\omega_{i_{\mathrm{n}}}l/\overline{V_{\mathrm{n}}}\right)^{5/3}} \tag{9}$$

where I=0.12, l=600 is the turbulence length scale; $\overline{V_{\mathrm{n}}}$ is the average wind speed.

2.4. Model constraints

Interval criteria are different in different countries or institutions due to differences in monitoring techniques or evaluation criteria. Two interval criteria based on wake vortex are adopted in the research, as shown in Table 1[44].

Table 1 Wake turbulence separation minima d_{IC}.

Front	CCAR-93-R5 category – ownership(km)				Front	RECAT-CN category – ownership(km)				
	J	H	M	L		J	B	C	M	L
J	5.6	11.1	13.0	14.8	J	4.7	9.3	11.1	13.0	14.8
H	5.6	7.4	9.3	11.1	B	4.7	5.6	7.4	9.3	13.0
M	5.6	5.6	5.6	9.3	C	4.7	4.7	4.7	6.5	11.1
L	5.6	5.6	5.6	5.6	M	4.7	4.7	4.7	4.7	9.3
					L	4.7	4.7	4.7	4.7	4.7

Note: CCAR represents China Civil Aviation Regulation; RECAT-CN represents Wake Turbulence Re-Categorization in China.

For safety reasons, aircraft must comply the performance limits and ATM speed constraints. The study adopts the IAS flight mode and $V_{\mathrm{I}} \in \left[V_{\mathrm{I,min}}, V_{\mathrm{I,max}}\right]$. Also, during speed adjustment, the maximum acceleration value is $a_{\mathrm{v,max}} = 2$ kt/s (1 kt=1.852 km/h).

3. Modeling of dynamic fuzzy speed control

This section describes the realization of IMS. We firstly introduce the operation flow of IMS. As the key algorithm of IMS, DFVD is described in detail later. Finally, the significant design parts of the decision algorithm are introduced.

3.1. Interval management system flow

Fig. 4 shows the flow of IMS for realizing IM by controlling the speed of aircraft sequence. Flight parameters used in DFVD include flight speed and flight distance. The uncertainty wind is generated by the model described in Section 2.3. During the *j*th time step, as the input parameters required for IM, $d_{i-1,i,j}$, $d_{i,i+1,j}$, $V_{\mathrm{T},i,i-1,j}$, and $a_{i-1,i,j}$ are calculated. After that, the speed adjustment value $\Delta V_{\mathrm{I},i,j}$ is decided based on DFVD. Once all aircraft in the current *j*th time unit have completed their decisions, aircraft will follow the speed decision with $\Delta \boldsymbol{V}_{\mathrm{I},j} = \left[\Delta V_{\mathrm{I},2,j}, \Delta V_{\mathrm{I},3,j}, ..., \Delta V_{\mathrm{I},N_{\mathrm{A}},j}\right]$ and the next time loop will be performed. The aircraft will be popped out as it flies through the final point. Once all aircraft are popped, the speed control is finished.

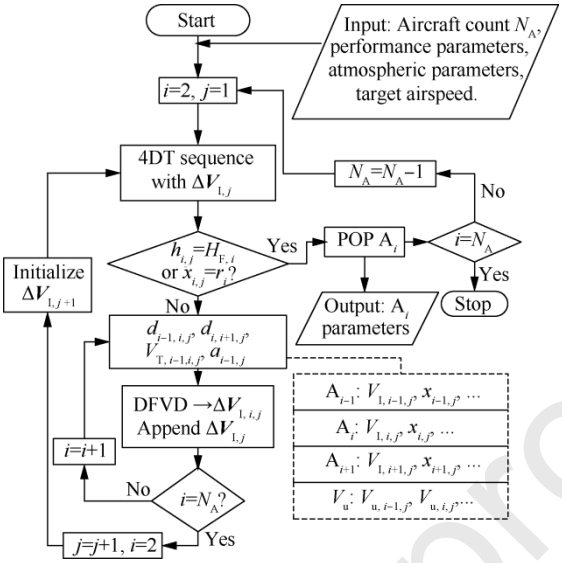

Fig. 4 Flowchart of IMS.

DFVD is the key link to decide speed adjustment, and the input parameters can be calculated as follows:

$$\begin{cases} d_{i-1,i,j} = x_{i-1,j} - x_{i,j} - 2d_{\mathrm{IC},i-1,i} \\ d_{i,i+1,j} = x_{i,j} - x_{i+1,j} - 2d_{\mathrm{IC},i,i+1} \\ V_{\mathrm{T},i,i-1,j} = V_{\mathrm{T},i,j} - V_{\mathrm{T},i-1,j} + V_{\mathrm{u},i-1,j} \\ a_{i-1,j} = V_{\mathrm{I},i-1,j} - V_{\mathrm{I},i-1,j} \end{cases} \tag{10}$$

3.2. Dynamic fuzzy velocity decision algorithm

The DFVD algorithm is designed for the speed adjusting decision of all aircraft. Iterate over each aircraft A_i (i=2, 3, …, N_A) in a time unit, and if the distance between A_i and A_{i-1} is greater than the maximum interval settings, then A_i directly adjust the speed according to the maximum acceleration $a_{v,\max}$. Otherwise, update the spacing between A_i and A_{i-1}, and A_i and A_{i+1} according to rows 9 and 10 of Algorithm 1 to ensure $d_{i-1,i} \in \left[0, k_1 d_{\mathrm{IC},i-1,i}\right]$ and $d_{i,i+1} \in \left[0, k_2 d_{\mathrm{IC},i,i+1}\right]$, where k_1 and k_2 are the corresponding bounds. Then dynamically generate the membership function and fuzzify (rows 12 and 13), perform rules (rows 14 and 15), aggregation and defuzzification (rows 16 and 17), and finally complete the speed regulation decision of an aircraft (row 18), until the speed adjusting decision is made for the aircraft sequence. The entire decision-making algorithm is shown as Algorithm 1.

Algorithm 1. DFVD algorithm for A_i (i=2, 3, …, N_A) in the jth time unit

1. Input: aircraft types, $d_{i-1,i,j}$, $d_{i,i+1,j}$, $V_{T,i,i-1,j}$, and $a_{i-1,j}$ calculated by Eq.(10)
2. Initialize: speed adjustment value $\Delta V_{1,i,j}$ and $\Delta \boldsymbol{V}_{1,j}$
3. Calculate $d_{IC,i-1,i}$ and $d_{IC,i,i+1}$ according to aircraft types
4. **For each** A_i in the aircraft sequence in the j^{th} time unit
5. **IF** $d_{i-1,i,j} > k_1 \bullet d_{IC,i-1,i}$
6. $\Delta V_{1,i,j} \leftarrow a_{v,max} \times \Delta t$
7. *continue*
8. **Else**
9. $d_{i-1,i,j} \leftarrow \min[\max(d_{i-1,i,j}, 0), k_1 \bullet d_{IC,i-1,i}]$
10. $d_{i,i+1,j} \leftarrow \min[\max(d_{i,i+1,j}, 0), k_2 \bullet d_{IC,i,i+1}]$
11. **End if**
12. Membership functions generation and fuzzification:
13. **return** membership values in the input linguistics
14. Fuzzy rules interface:
15. **return** membership values in the output linguistics
16. Aggregation and defuzzification:
17. **return** $\Delta V_{1,i,j}$
18. Append $\Delta \boldsymbol{V}_{1,j}$ with $\min[\max(\Delta V_{1,i,j}, -\Delta t \bullet a_{v,max}), \Delta t \bullet a_{v,max}]$
19. **End for**
20. Output: $\Delta \boldsymbol{V}_{1,j}$

The DFVD algorithm mainly includes three key sections: fuzzification based on membership function, fuzzy inference based on rules, and aggregation and defuzzification. These three primary steps are in rows 12-17 of Algorithm 1, which are specifically described from Section 3.3 to Section 3.5.

3.3. Dynamic fuzzification

The dynamic characteristics of the fuzzification process are reflected in two aspects. Dynamically generate the membership bounds of universe of discourses, based on (A) different d_{IC} between adjacent aircraft and (B) the limitation of the TAS in real-time altitude.

In fuzzy theory, a universe of discourse (U) is usually divided into multiple elements scaled fuzzy sets. Fuzzification is the process of determining how true an input variable belongs to a fuzzy set. This truth degree is membership. It is a major task to define membership functions to realize dynamic property. Although trapezoidal and triangular membership functions are quite simple and have been used extensively in many applications[33], we chose bell-shaped (F_{B}), S-shaped (F_{S}), and Z-shaped (F_{Z}) functions according to the result of the pre-research. The expressions of these shapes are given as follows:

$$F_{\mathrm{B}}\left(x;a_1,a_2,a_3\right)=1\Big/\left[1+\left(x-a_3\right)^{2a_2}\cdot a_1^{-2a_2}\right] \tag{11}$$

$$F_{\mathrm{S}}\left(x;a_4,a_5\right)=\begin{cases}0 & x\le a_4\\ 2\left(\dfrac{x-a_4}{a_5-a_4}\right)^2 & a_4<x\le\dfrac{a_4+a_5}{2}\\ 1-2\left(\dfrac{x-a_4}{a_5-a_4}\right)^2 & \dfrac{a_4+a_5}{2}<x\le a_5\\ 1 & x>a_5\end{cases} \tag{12}$$

$$F_{\mathrm{Z}}\left(x;a_6,a_7\right)=1-F_{\mathrm{S}}\left(x;a_6,a_7\right) \tag{13}$$

Significant parameters that affect the safety interval in an aircraft sequence are the distance between the front and the current aircraft (U_{f}), the distance between the current and the rear aircraft (U_{r}), the relative TAS between the front and the current aircraft (U_{v}), and the acceleration of the front aircraft (U_{a}). These four parts are the universe of discourse of inputs. The fuzzy set in each universe concept are: U_{f} = {Near, Middle, Far}, U_{r} = {Near, Far}, U_{v} = {Slow, Fast}, U_{a} = {Decelerate, Accelerate}. We construct the input membership functions with parameters k_1=k_2=4, k_3=0, k_4=1.5, k_5=3, as shown in Figs. 5 (a)-(d).

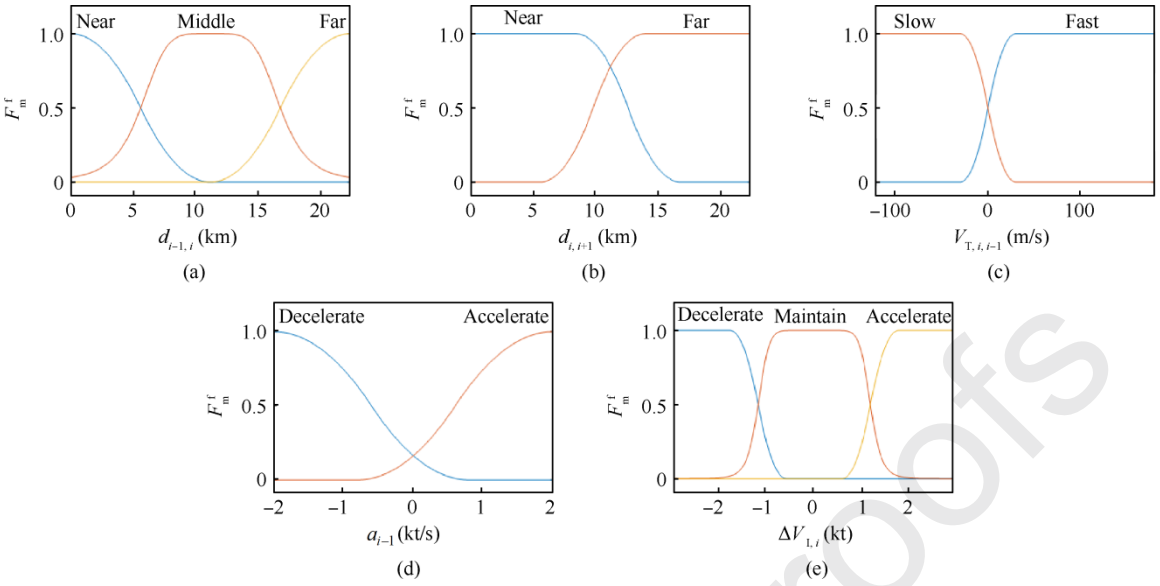

Fig. 5 Membership functions.

Controlling flight speed is a primary strategy for managing intervals. The variation value of the current aircraft IAS is the output universe of discourse and defined as U_o = {Decelerate, Maintain, Accelerate}, as shown in Fig. 5 (e). There follow the specific generation methods for the membership functions.

Fig. 5(a) shows the membership functions of $d_{i-1,i}$, which derive from Eqs.(11)-(13). In detail, $F^{f}_{m,near}\left(d_{i-1,i}\right)=F_Z\left(d_{i-1,i};k_3\cdot d_{IC,i\text{-}1,i},k_1/2\cdot d_{IC,i\text{-}1,i}\right)$, $F^{f}_{m,mid}\left(d_{i-1,i}\right)=F_B\left(d_{i-1,i};d_{IC,i\text{-}1,i},2.5,2d_{IC,i\text{-}1,i}\right)$, $F^{f}_{m,far}\left(d_{i-1,i}\right)=F_S\left(d_{i-1,i};k_1/2\cdot d_{IC,i\text{-}1,i},\left(k_1-k_3\right)d_{IC,i\text{-}1,i}\right)$. The interval criterion $d_{IC,i\text{-}1,i}$ changes with the $(i-1)$th or ith aircraft type, which leads to a dynamic generation of membership functions in the universe of discourse of U_f.

Fig. 5 (b) shows the membership functions of $d_{i,i+1}$ derived from Eqs.(11) and (13). In detail, $F^{r}_{m,near}\left(d_{i,i+1}\right)=F_Z\left(d_{i,i+1};k_4\cdot d_{IC,i,i+1},k_5\cdot d_{IC,i,i+1}\right)$, $F^{r}_{m,far}\left(d_{i,i+1}\right)=F_S\left(d_{i,i+1};\left(k_2-k_5\right)d_{IC,i,i+1},\left(k_2-k_4\right)d_{IC,i,i+1}\right)$. Similar with the universe of discourse of U_f, the membership functions of U_r are dynamically generated by different combinations of the ith and $(i-1)$th aircraft type.

The membership functions of relative TAS between two aircraft are shown in Fig. 5(c). Denote $V^{R}_{T}=V^{R}_{T,max}-V^{R}_{T,min}$ and $V_{T,i,i\text{-}1}\in\left[V^{R}_{T,min},V^{R}_{T,max}\right]$, where $V^{R}_{T,min}$ is the minimum TAS of A_i minus the maximum TAS of A_{i-1} and $V^{R}_{T,max}$ is the maximum TAS of A_i minus the minimum TAS of A_{i-1}. The membership functions can be expressed as: $F^{v}_{m,slow}\left(V_{T,i,i\text{-}1}\right)=F_S\left(V_{T,i,i\text{-}1};-0.1V^{R}_{T},0.1V^{R}_{T}\right)$, $F^{v}_{m,fast}\left(V_{T,i,i\text{-}1}\right)=F_Z\left(V_{T,i,i\text{-}1};-0.1V^{R}_{T},0.1V^{R}_{T}\right)$. During the en-route descent process, the limitation of IAS for an aircraft is constant. Within a decision cycle, $V^{R}_{T,min}$ and $V^{R}_{T,max}$ can be calculated according to IAS limitations and real-time flight altitude of aircraft based on Eq.(3). V^{R}_{T} that changes in real time could be obtained subsequently, which leads to generating the membership functions of U_v dynamically.

The acceleration membership function is generated statically, since the constraint is described in Section 2.4. Fig. 5(d) shows the membership functions of $a_{i-1} \in \left[-a_{\mathrm{v,max}},\ a_{\mathrm{v,max}}\right]$, $F^{\mathrm{a}}_{\mathrm{m,dec}}\left(a_{i\text{-}1}\right) = F_{\mathrm{Z}}\left(a_{i\text{-}1}\ ; -a_{\mathrm{v,max}}\ , 0.8\right)$, $F^{\mathrm{a}}_{\mathrm{m,acc}}\left(a_{i\text{-}1}\right) = F_{\mathrm{S}}\left(a_{i\text{-}1}\ ; -0.8\ , a_{\mathrm{v,max}}\right)$.

Fig. 5(e) shows the speed adjustment membership function of the current aircraft, as the output is statically fuzzified into three fuzzy sets. The range of speed change is preset as $\Delta V_{\mathrm{I},i} \in [-3,\ 3]$ kt. The membership functions of output fuzzy sets are $F^{\mathrm{a}}_{\mathrm{m,dec}}\left(\Delta V_{\mathrm{I},i}\right) = F_{\mathrm{Z}}\left(\Delta V_{\mathrm{I},i}\ ; -1.8\ , -0.6\right)$, $F^{\mathrm{a}}_{\mathrm{m,mid}}\left(\Delta V_{\mathrm{I},i}\right) = F_{\mathrm{B}}\left(\Delta V_{\mathrm{I},i}\ ; 1.2\ , 5\ , 0\right)$, $F^{\mathrm{a}}_{\mathrm{m,acc}}\left(\Delta V_{\mathrm{I},i}\right) = F_{\mathrm{S}}\left(\Delta V_{\mathrm{I},i}\ ; 0.6\ , 1.8\right)$.

3.4. Fuzzification rules and interface

After fuzzifying inputs, we obtain the truth degrees of the observations for different fuzzy sets in different universes of discourses. But these membership values cannot establish a direct relationship with output variables. Inference based on fuzzy rules can determine this implied relationship. Table 2 shows the fuzzy rules, and " - ", "○", and "+" represent the universes of discourses of deceleration, maintenance, and acceleration, respectively.

Table 2 Fuzzification rules.

U_{v}	U_{a}	U_{f}	Near		Middle		Far	
		U_{r}	Near	Far	Near	Far	Near	Far
Fast	Decelerate		+	-	○	-	+	+
	Accelerate		○	-	○	○	+	+
Slow	Decelerate		○	-	○	○	+	+
	Accelerate		-	-	+	○	+	+

The inference process is realized using "IF … THEN" conditional statements connected with the fuzzy AND operator. Taking A_i as an example, the inference logic for the 3rd row and 4th column in Table 2 is given as follows:

IF ($d_{i-1,i}$ is near AND $d_{i,i+1}$ is near AND $V_{\mathrm{T},i,i\text{-}1}$ is fast AND $a_{i\text{-}1}$ decelerates)

THEN $\Delta V_{\mathrm{I},i}$ decelerates

3.5. Aggregation and defuzzification

A membership value will be obtained after a rule is operated as previous statement. Using this value to truncate the output membership function will obtain a new truncated function. A set of inputs may be meaningful under multiple rule actions, so all rules should be tested. This will result in generating a set of truncation functions. We set the weight of each rule to be 1 and use the OR operator to integrate truncated output membership functions. After OR operation, we will obtain one integrated membership function.

Then, we use the centroid average method to defuzzify, and transform the language term into an accurate output value. The essence of the centroid method is to calculate the centroid of the integrated membership function. Fig. 6 depicts the defuzzification effects with $V_{\mathrm{T},i,i-1} = -40$ (1st row), 0 (2nd row), 40 (3rd row) m/s and $a_{i-1} = -1$ (1st column), 0 (2nd column), 1 (3rd column) kt/s, respectively. The parameters of membership functions are the same as those in Fig.5. The maximum of $\Delta V_{\mathrm{I},i}$ in Fig. 6 (a) is 1.65 kt, and that in Fig. 6 (i) is minimum with –1.9 kt. This effect conforms to the fuzzy rule settings in Table 2. It can be seen from the figure that there are many conditions in which it is not necessary to change the flight speed.

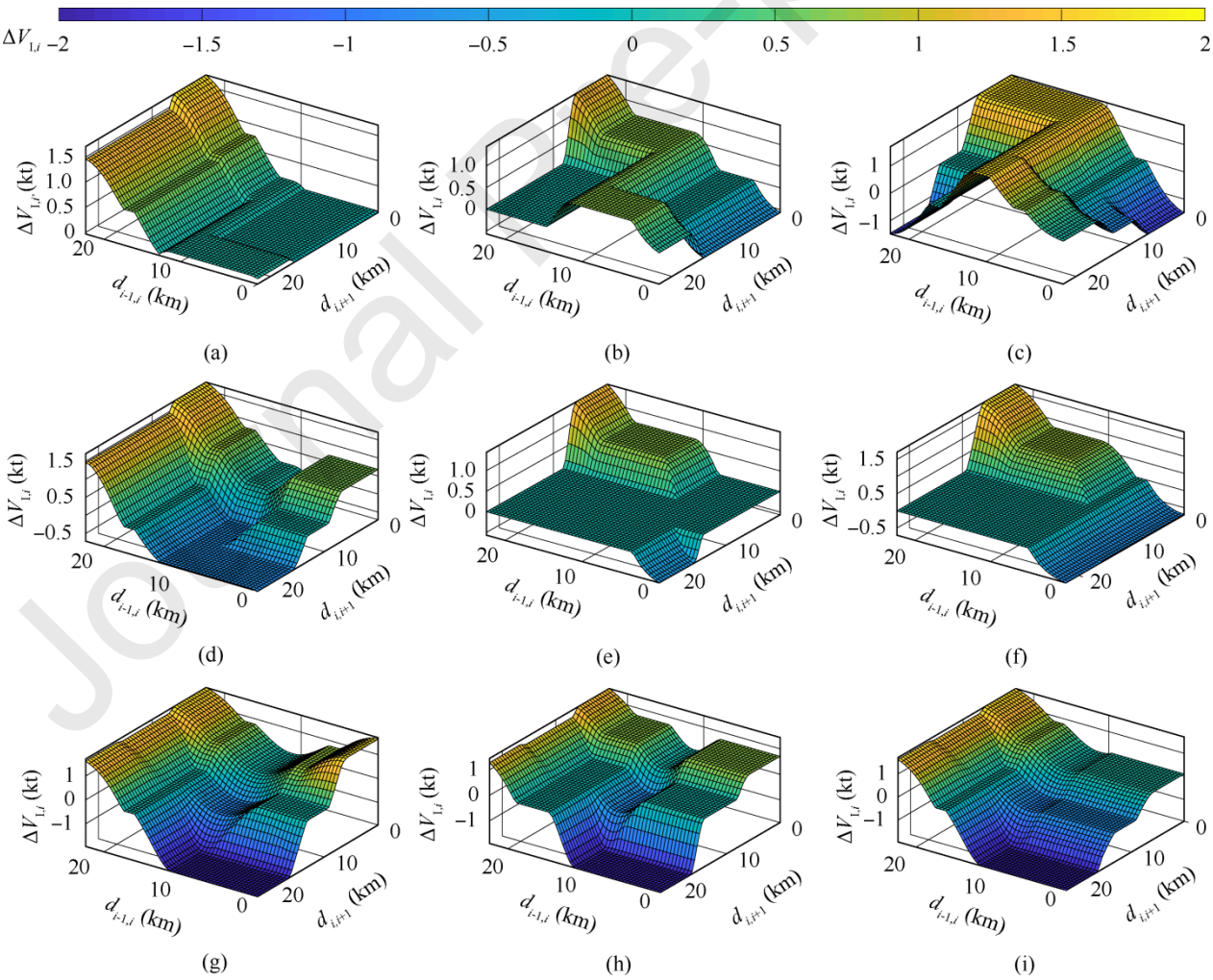

Fig. 6 Defuzzification effects under different $V_{\mathrm{T},i-1,i}$ and a_{i-1}.

4. Simulation results and analysis

In this section, we evaluate the proposed IMS prototype based on both actual and simulated flight data and analyze the results. Firstly, we set up the experimental scenarios and assumptions, as well as introduce the actual flight trajectory. Then, we formulate the evaluation indicators. After that, we verify the effectiveness and the uncertainty suppression of the proposed algorithm. Finally, we analyze the influencing factors of the results. The proposed prototype was developed in C# and tests were performed using a single machine (Intel(R) Core(TM) i7-1065G7, core processor (1.3 GHz), and 8 GB RAM).

4.1. Scenario and assumptions

4.1.1. Overview

The initial flight height during the en-route descent process is $H_S = 8\ \mathrm{km}$. Aircraft are assumed to be in level flight before TOD and using continuous descent operation after the point. The entire process adopts IAS flight. The total flight range $r_i = 150\ \mathrm{km}$ and the end height $H_F = 2\ \mathrm{km}$. The experimental setup follows these conditions:

(1) IDLE thrust with standard atmosphere condition.

(2) The first aircraft in the test adopts real flight data or flies in a uniform deceleration mode depending on the case.

(3) ATM speed limitation is $\left[V_{\mathrm{ATM,min}}, V_{\mathrm{ATM,max}}\right] = \left[130\ \mathrm{kt}, V_{\mathrm{I,max}} - 30\ \mathrm{kt}\right]$.

(4) Initial V_{I} is generated randomly in $\left[V_{\mathrm{I,min}} - 100\ \mathrm{kt}, V_{\mathrm{I,max}} - 70\ \mathrm{kt}\right]$.

(5) Target IAS $V_{\mathrm{Tg},i}$ is generated randomly in $\left[V_{\mathrm{ATM,min}} + 30\ \mathrm{kt}, V_{\mathrm{ATM,max}} + 90\ \mathrm{kt}\right]$.

(6) Initial interval is the same with actual spacing data or generated randomly in [2, 6]• $d_{\mathrm{IC},i\text{-}1,i}$, depending on the case.

(7) If an aircraft becomes the first one, adjust V_{I} to $V_{\mathrm{Tg},i}$ with $\pm a_{\mathrm{v,max}}$ until passing the endpoint with $V_{\mathrm{Tg},i}$.

(8) When the first aircraft enters the airspace, the clock is reset to zero.

(9) To avoid accidental error, each case carries out 10 runs except the experiment in Sections 4.3.1 and 4.4.

Aircraft types and speed limitations based on performance are shown in Table 3, as well as the aircraft category.

Table 3 Aircraft and parameters.

Aircraft type	Category CCAR	Category RECAT	$V_{I,min}$ (kt)	$V_{I,max}$ (kt)
A320	M	M	105	350
A321	M	M	106	350
A330	H	B	106	330
A350	H	B	116	340
A380	J	J	117	340
B738	M	M	105	340
B752	H	M	116	350
B772	H	B	111	330
B788	H	B	118	360
G650	M	M	104	340

The 3000 s uncertainty simulated wind (sample) used in the study is shown in Fig. 7.

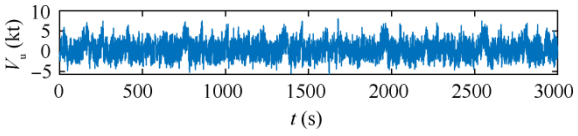

Fig. 7 Uncertainty wind speed sample.

4.1.2. Actual flight data

The actual flight data are used to verify the effectiveness of the algorithm. We downloaded the arrival flight states of Heathrow Airport (LHR) on 2022-06-27 from OpenSky, and filtered and preprocessed the flight sequence according to the following principles:

(1) Aircraft continuous flight sequence includes 3 aircraft at least, which are not affected by other flights.

(2) Each aircraft uses the same STAR or intercepts the same approach procedure.

(3) No more than 5% missing data during the descent process from $H_S = 8$ km to $H_F = 2$ km.

(4) Linearly interpolate the data based on 1 s.

(5) Inversely derive flight parameters before TOD during level flight with height 8 km.

The actual flight trajectories consisting of longitude and latitude profiles and vertical profiles are shown in Figs. 8 (a) and (b), respectively.

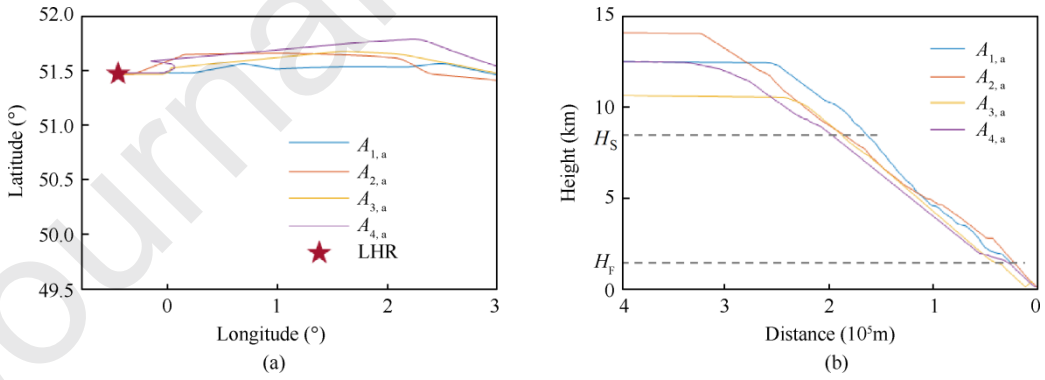

Fig. 8 Actual flight trajectories of aircraft $A_{i,a}$.

The abscissa in Fig. 8 (b) represents the flight distance of the aircraft from LHR. The descent trajectories between the two dashed lines are the experimental segments. The flight process above H_S is assumed to be a level flight at this height.

It should be noted that this group of real trajectories starts with $A_{2,a}$ flying ahead of $A_{1,a}$, but according to the approach sequence, $A_{1,a}$ will finally fly past $A_{2,a}$. We assume that $A_{1,a}$ and $A_{2,a}$ do not conflict during descent. Several

significant parameters related to the experiment of the actual data are shown in Table 4. Unless otherwise stated, the above scenarios are applicable to all experiments.

Table 4 Aircraft flight sequence information.

Number	Flight number	Aircraft type	Initial V_1(kt)	$V_{\mathrm{Tg},i}$ (kt)
$A_{1,\mathrm{a}}$	MH2	A350	264	208
$A_{2,\mathrm{a}}$	QQE569	G650	237	166
$A_{3,\mathrm{a}}$	QR8854	B773	270	173
$A_{4,\mathrm{a}}$	BA32	B789	244	226

4.2. Evaluation indicators

The following indicators are defined to evaluate and analyze the experimental results:

(1) Separation rate R_{S} and its average value $\overline{R_{\mathrm{S}}}$

R_{S} represents the spacing ratio between two adjacent aircraft and the interval criterion in m numbers of time unit. $\overline{R_{\mathrm{S}}}$ is the average value of R_{S} for all adjacent aircraft pairs in all numbers of runs, shown as follows:

$$R_{\mathrm{S},i-1,i}=\sum_{j=1}^{m}\frac{d_{i-1,i,j}}{m\cdot d_{\mathrm{IC},i-1,i}} \tag{14}$$

(2) IC deviation rate $R_{\mathrm{D},k}$ and its average value $\overline{R_{\mathrm{D},k}}$

$R_{\mathrm{D},k}$ ($k\geq 1$ denoted as the deviation coefficient) is the ratio of the two aircraft's flight time with the separation between $\left[(k-1)\cdot d_{\mathrm{IC},i\text{-}1,i}\ ,\ k\cdot d_{\mathrm{IC},i\text{-}1,i}\right]$ to the total common flight time ($t_{\mathrm{T},i\text{-}1,i}$) of $A_{i\text{-}1}$ and A_i. $\overline{R_{\mathrm{D},k}}$ represent the average value of $R_{\mathrm{D},k}$ for all adjacent aircraft combinations in every moment during all runs, which can be expressed as follows:

$$R_{\mathrm{D},k,i\text{-}1,i}=\frac{t\left|_{d_{i\text{-}1,i}\in\left[(k-1)\cdot d_{\mathrm{IC},i\text{-}1,i},\,k\cdot d_{\mathrm{IC},i\text{-}1,i}\right]}\right.}{t_{\mathrm{T},i\text{-}1,i}} \tag{15}$$

(3) Total en-route descent time T_{ED} and its average value $\overline{T_{\mathrm{ED}}}$

T_{ED} means the total flight time of a sequence managed by IMS, which starts when the first aircraft in the sequence takes control and ends when the last aircraft finishes control. $\overline{T_{\mathrm{ED}}}$ is the average value of T_{ED} for all runs.

(4) Average speed $\overline{V_{\mathrm{I}}}$

$\overline{V_{\mathrm{I}}}$ represents the average of $V_{\mathrm{I},i}$ for all aircraft in all runs.

4.3. Effectiveness verification

To verify the effectiveness of the proposed IMS, we compare the result of the experiment using the system prototype with the actual flight data introduced in Section 4.1.2. To further verify the effectiveness and stability with different operating scenarios, we introduce a complex simulation environment that meets the conditions in Section 4.1.1, execute the prototype and record results.

4.3.1. Verification based on actual data

The first aircraft in the experimental group adopts the actual data of $A_{1,\mathrm{a}}$, the initial and end conditions of the remaining aircraft are the same as the actual data of $A_{2,\mathrm{a}}$ – $A_{4,\mathrm{a}}$, and then the DFVD algorithm is used to solve and calculate IAS, trajectories, flight parameters, and indicators. The experiments are assumed to be carried out under standard atmospheric and calm wind conditions.

Results generated by DFVD are shown in Figs. 9 (a)-(d) and marked as A_1 – A_4. $A_{1,\mathrm{a}}$ – $A_{4,\mathrm{a}}$ are the control group with actual data. The descending vertical profiles in Fig. 9 (a) of the experimental and control groups are similar. Figs. 9 (b) and (c) clearly depict the trend of flight height and distance over time. From Figs. 9 (a) to (c), we find that the whole descending process is safe. The initial and ending IAS in Fig. 9 (d) is the same for these two groups. Therefore, the DFVD proposed in this paper can effectively solve the automatic interval management in the multi-aircraft operation process. Fig. 9 (d) shows that A_2 – A_4 can adjust the IAS faster with lower frequency compared with $A_{2,\mathrm{a}}$ – $A_{4,\mathrm{a}}$. In Fig. 9 (e), the scale 1 on the vertical axis represents that the spacing between the adjacent aircraft equals to the interval criterion, $d_{1,2}$ surpasses the safe interval after 148 s, while $d_{3,4,\mathrm{a}}$ is less than the interval after 1989 s. This result indicates that the capability of IM is greatly improved, which is specifically recorded in the following indicator comparison table.

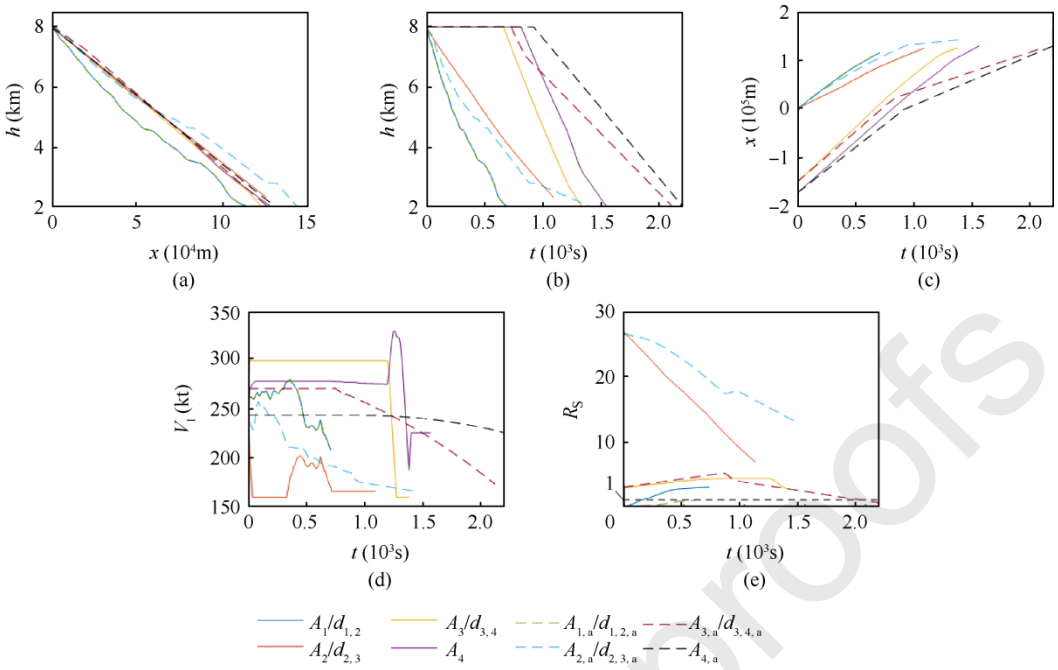

Fig. 9 Actual flight data and results using IMS.

Combining Fig. 9(e) (marked as $d_{i\text{-}1,\,i}$ for DFVD results and $d_{i\text{-}1,\,i,\mathrm{a}}$ for the control group) and Table 5, we can find that the IMS can quickly reduce the distance between two aircraft with large spacings ($d_{2,3}$) and rapidly increase the distance in the opposite case ($d_{1,2}$). If the distance between two aircraft reduces, IMS can avoid the spacing shorter than the safety interval ($d_{3,4}$). T_{D}=4788 s in the actual data, and this parameter reduced to 3353 s (reduced by 29.97%) after using IMS. The results show that IMS improves the en-route descent efficiency while ensuring safety.

Table 5 Indicator comparison for distance between adjacent aircraft.

Number	$R_{\mathrm{S},i\text{-}1,i}$	$R_{\mathrm{D},1}$	$R_{\mathrm{D},2}$	$R_{\mathrm{D},3}$	$R_{\mathrm{D},4}$	$R_{\mathrm{D},5}$	$R_{\mathrm{D},6}$	$R_{\mathrm{D},7}$
$d_{1,2}$	2.0867	0.2079	0.2135	0.2781	0.3006	0	0	0
$d_{2,3}$	15.8182	0	0	0	0	0	0.0441	0.9559
$d_{3,4}$	3.8969	0	0	0.0770	0.4014	0.5216	0	0
$d_{1,2,\mathrm{a}}$	0.5676	0.8336	0.1664	0	0	0	0	0
$d_{2,3,\mathrm{a}}$	20.1332	0	0	0	0	0	0	1
$d_{3,4,\mathrm{a}}$	3.1444	0.0587	0.1660	0.1665	0.3411	0.2148	0.0530	0

4.3.2. Verification based on random simulation data

The flight sequence in this experiment consists of 20 aircraft (N_A=20). Except for the first one, aircraft are randomly generated based on the types shown in Table 4. $A_{1,a}$ in Table 4 is set as the first aircraft in control experiment and $r_i = 150$ km. Other experimental conditions are set according to the rules in Section 4.1.1. The level flight distance and descent distance are calculated by Eqs.(1)-(4).

Fig. 10 shows the results of one run, where Figs. 10 (a)-(d) marked as $A_1 - A_{20}$ and Fig. 10 (e) marked as $d_{i\text{-}1,\,i}$. The TOD point of each aircraft is different in Fig. 10 (a), which leads to different descent rates. Figs. 10 (b) and (c) show the coordinate plots of flight altitude and distance versus time, respectively. From Figs. 10 (a) to (c), we can find that at every moment the descending process of the sequence is safe. The adjustment process of IAS is shown in Fig. 10 (d). Speed adjustment is frequent at the beginning, and then tends to slow down. The intervals between two adjacent aircraft in Fig. 10 (e) meet the safety standards.

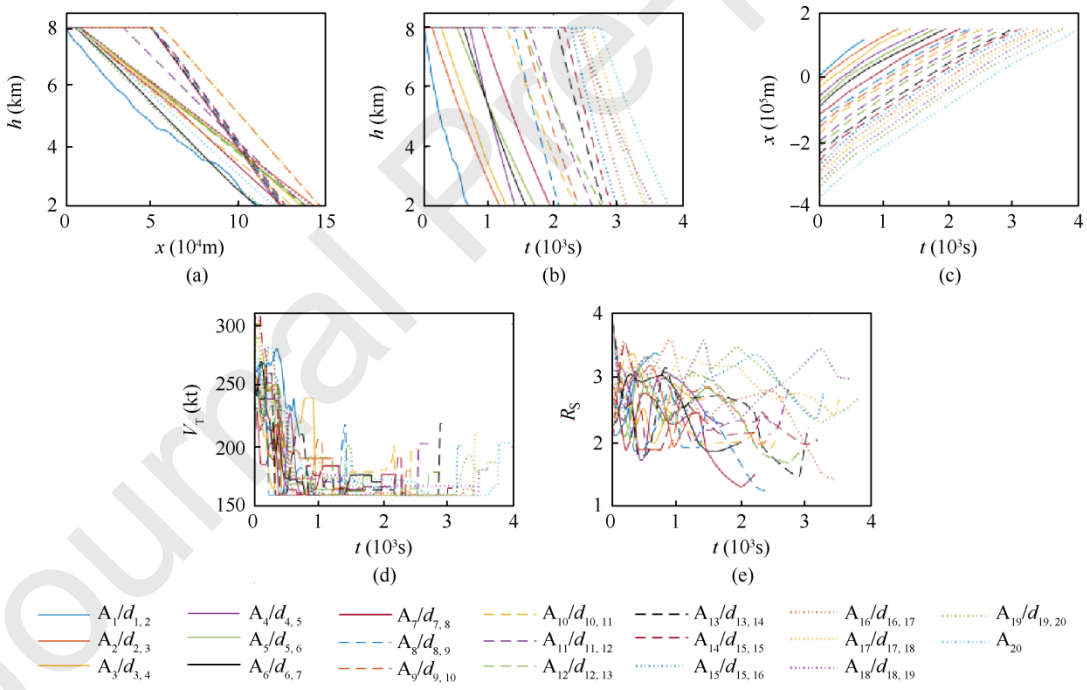

Fig. 10 Simulation data and results using IMS.

The average value of interval evaluation indicators for 10 runs are shown in Table 6. The average separation rate is 2.7256, with an average of 61.44% separation values distributed between [2, 3] d_{IC}. The spacing of less than 0.2% is smaller than the criterion and the adjustment time is a few seconds. The average value of total en-route descent time for 20 aircraft is 4255 s.

Table 6 Indicators between adjacent aircraft for simulation experiment.

$\overline{R_S}$	$\overline{T_{ED}}$ (s)	$\overline{V_I}$ (kt)	$\overline{R_{D,1}}$	$\overline{R_{D,2}}$	$\overline{R_{D,3}}$	$\overline{R_{D,4}}$	$\overline{R_{D,5}}$	$\overline{R_{D,6}}$	$\overline{R_{D,7}}$
2.7256	4255	185.8	0.0013	0.0709	0.6130	0.2994	0.0090	0.0036	0.0028

The verification results in Section 4.3 prove that the proposed prototype system can operate stably in different operating scenarios, even in a more complex environment than the actual one.

4.4. Uncertainty suppression verification

The experimental setup in this section is based on Section 4.3.1, while the uncertainty is added. We designed two control groups to verify the uncertain suppression performance. For the first control group, we assume that $A_2 - A_4$ fly at a uniform deceleration (–0.1 kt/s), denoted as the Unf-group and marked with subscript "u". For the second control group, we designed $A_2 - A_4$ to follow the speed change of A_1, denoted as the Flw-group and marked with subscript "f". The wind change directly leads to the V_I change in this group. The experimental group disposes of the uncertainty wind by DFVD.

As shown in Figs. 11 (a)-(c), the vertical profiles of the aircraft in the same order are similar for the three methods, as well as the coordinate plots of flight altitude and distance versus time, while the change of V_I is quite different (Fig. 11 (d)). V_I in the Unf-group changes smoothly because the acceleration is constant before the aircraft reaches the target IAS. The trend of V_I in the Flw-group changes according to the first aircraft, while a little deviation is caused by uncertainty wind. This deviation is insignificant relative to the wind, which means that this method can reduce the influence of uncertainty to some extent, but the fluctuation of IAS is obvious. Meanwhile, these two methods lack the judgment and adjustment of the distance between adjacent aircraft, which results in unreasonable spacing. By comparing the results in Section 4.3 and this section, it can be found that the trends of V_I and R_S are almost the same. Therefore, uncertainty winds have little effect on the result of IMS.

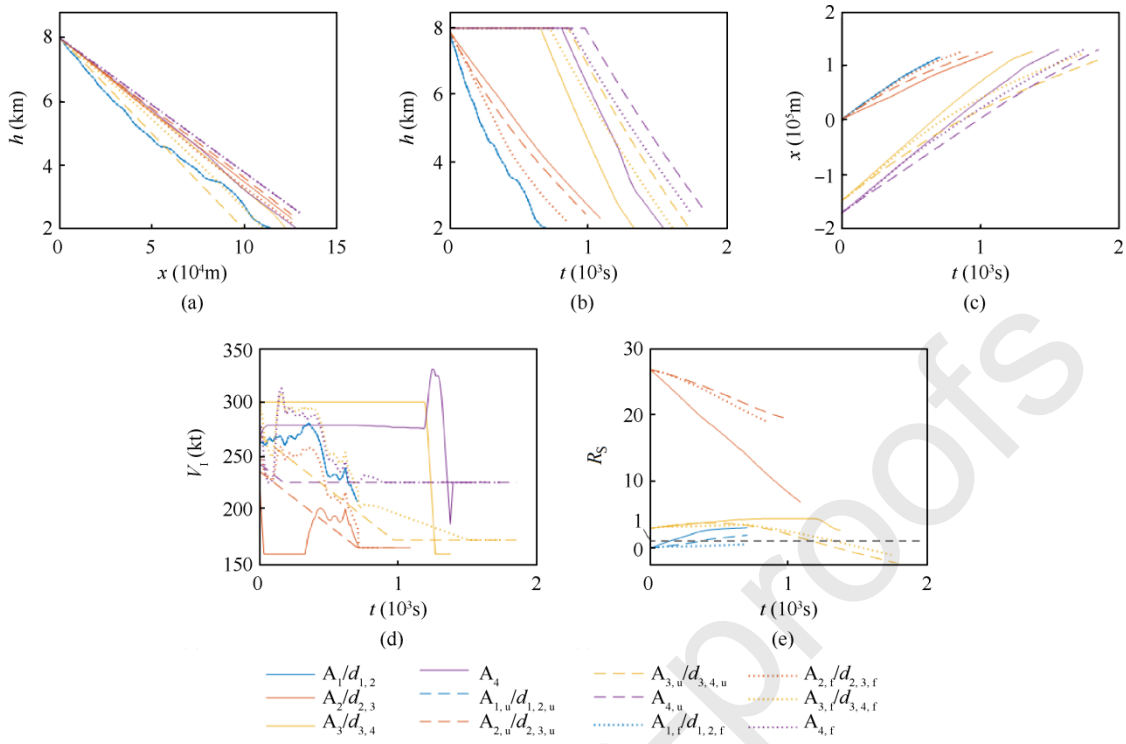

Fig. 11 Results with wind uncertainty.

4.5. Sensitivity study and analysis

In this section, we analyze the sensitivity of DFVD for interval management results. The bounds and parameters of membership functions for U_f and U_r primarily affect the spacing results, which we specifically analyzed. Taking the experiment of Section 4.3.2 as the baseline of this section, the following experiments are set the same as the baseline if not otherwise specified.

4.5.1. Impacts of velocity membership functions bounds

To verify the advantage of dynamically generating the bounds of velocity membership functions, the variation range of $V_{T,i,i-1}$ is fixed as $\left[V^{R}_{T,min}, V^{R}_{T,max}\right]$=[–142, 145] m/s in the experimental group. Results are shown in Table 7. Compared with Table 6, the fixed bounds of U_v reduce $\overline{R_S}$ and $\overline{T_{ED}}$ with a faster $\overline{V_I}$. However, $\overline{R_{D,1}}$ with a static bound is 9 times that with a dynamic bound, and it will cause the rear aircraft to surpass the front one by using static bounds. In addition, it takes a long time and a large speed change to return to an acceptable interval level, which is unacceptable in practical operation. What's more, the case of $\overline{R_{D,k}}$ $(k > 4)$ occurs less frequently under the dynamic bounds compared with the baseline.

Table 7 Indicators between adjacent aircraft for fixed velocity membership functions.

$\overline{R_S}$	$\overline{T_{ED}}$ (s)	$\overline{V_I}$ (kt)	$\overline{R_{D,1}}$	$\overline{R_{D,2}}$	$\overline{R_{D,3}}$	$\overline{R_{D,4}}$	$\overline{R_{D,5}}$	$\overline{R_{D,6}}$	$\overline{R_{D,7}}$
2.6293	3447	191.5	0.0116	0.1289	0.5855	0.2460	0.0171	0.0077	0.0032

We take the velocity membership function as an example to illustrate the advantage of the dynamic generation method. Table 8 illustrates two different aircraft combination groups, based on which we carried on the experiment.

Table 8 Combinations for two adjacent aircraft with different types.

Group	Front aircraft A_{i-1}		Owner aircraft A_i	
	type	$[V_{I,min}, V_{I,max}]$ (kt)	type	$[V_{I,min}, V_{I,max}]$ (kt)
1	A320	[105, 350]	A320	[105, 350]
2	B788	[118, 350]	G650	[104, 340]

Table 9 shows the changes of $\left[V_{T,min}^{R}, V_{T,max}^{R}\right]$ for the two groups. From the table, it can be found that the combination of aircraft types and flight altitudes of adjacent aircraft will cause a huge difference in $\left[V_{T,min}^{R}, V_{T,max}^{R}\right]$. If static membership functions are used as the basis for decision-making, it will cause huge unstable factors. For example, a same combination of aircraft type with the same TAS will produce the same results when making decisions at different flight altitudes, while the TAS limitations have already changed, which leads to insecurity and instability decision. Differently, the dynamic membership functions will change over $\left[V_{T,min}^{R}, V_{T,max}^{R}\right]$, which leads to fair judgment for the current flight TAS. This insecurity and instability can be avoided by adopting the proposed DFVD method without adding fuzzy rules. Therefore, dynamically generating the U_v membership bounds does have advantages in terms of safety and stability.

Table 9 $\left[V_{T,min}^{R}, V_{T,max}^{R}\right]$ change with different altitude.

Group	$\left[V_{T,min}^{R}, V_{T,max}^{R}\right]$ (m/s)					
$[h_i, h_{i-1}]$ (km)	[8, 8]	[8, 7]	[7, 6]	[6, 5]	[5, 4]	[4, 3]
1	[-179, 179]	[-167, 183]	[-160, 175]	[-153, 168]	[-147, 160]	[-140, 153]

2	[-162, 180]	[-150, 184]	[-144, 176]	[-138, 168]	[-132, 161]	[-126, 154]

4.5.2. Impacts of distance membership functions bounds

Based on the baseline experiment, we change the bounds value of U_f (k_1) and U_r (k_2) membership functions. The vertical profile, flight speed, and R_S are similar with those in Fig. 10, as well as the coordinate plots of altitude and distance versus time. Statistical results of $\overline{R_S}$ ("○" in subfigure a), $\overline{T_{ED}}$ ("•" in subfigure b), and $R_{D,k}$ are shown in Figs. 12 and 13. The black point "•" in the Figs. 12 and 13 (b)-(f) represent $\overline{R_{D,k}}$.

Fig. 12 shows the effect of k_1 on the results. $\overline{R_S}$ has an overall increasing trend as k_1 increases (subfigure a). This is mainly because when the initial interval is large and the value of k_1 is small, $d_{i-1,i}$ belongs to "far" more often in the fuzzification process. As a result, $V_{I,i}$ increases and spacing between the current and the front aircraft decreases, and vice versa. The Figs. 12 (b)-(f) also reflect this change, and with the increase of k_1, $R_{D,1}$ and $R_{D,2}$ decrease while $R_{D,3}$ and $R_{D,4}$ increase significantly. The peak value of $R_{D,k}$ changes from k=3 to k=4. Due to performance limitations, fuzzy logic rules, and the DFVD algorithm, $\overline{R_S}$ will not increase or decrease indefinitely. It remains around [2.4, 3.2] d_{IC}. The distance between the two aircraft is rarely less than d_{IC} or greater than 5 d_{IC}. Conversely, the same is true when the value of k_1 is larger.

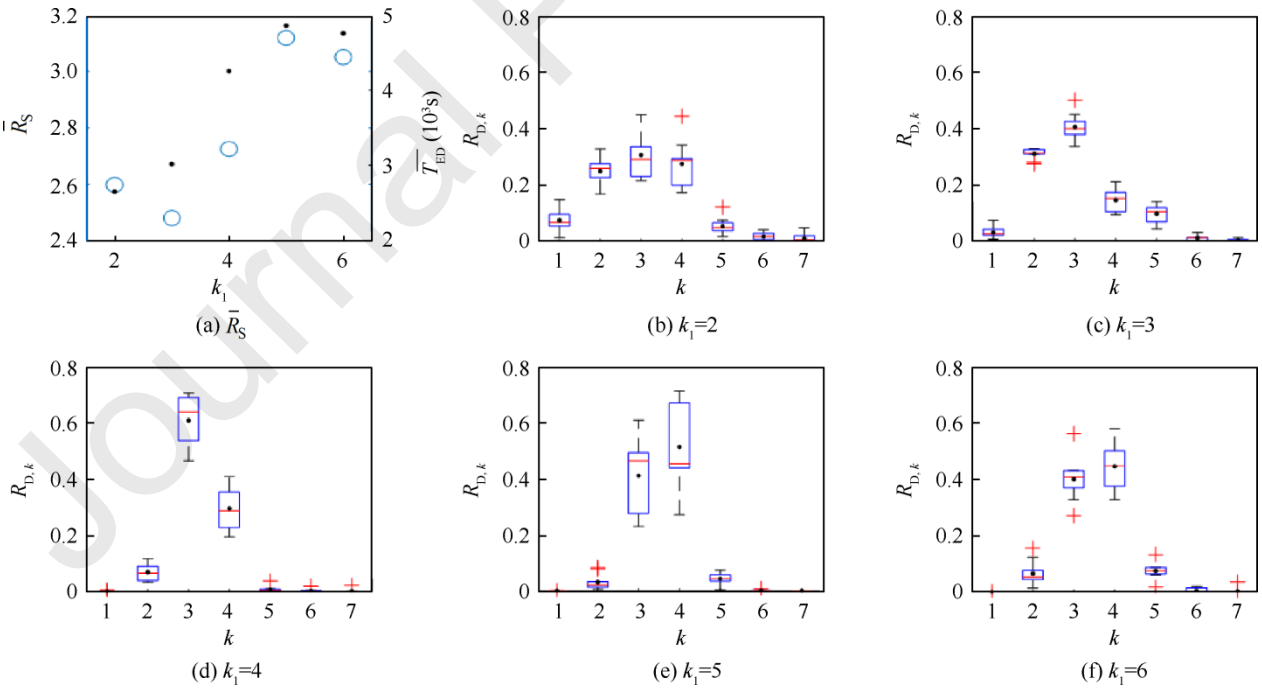

Fig. 12 Results of k_1 impacts on indicators.

The trend of $\overline{T_{ED}}$ is similar with $\overline{R_S}$, because under the same average descent speed, the larger the spacing between aircraft, the longer the flight time. However, $\overline{R_S}$ (k_1=2) is smaller than $\overline{R_S}$ (k_1=3), which is mainly caused by the faster average speed of each aircraft during the descent process with k_1=3, as shown in Table 10.

Table 10 $\overline{V_I}$ results under different k_1, k_2, and k_3.

Value	k_1					k_2					k_3				
	2	3	4	5	6	2	3	4	5	6	0	0.4	0.8	1.2	1.6
$\overline{V_I}$ (kt)	288.1	251.5	185.8	168.0	165.3	200.5	183.2	185.8	221.0	223.1	174.2	176.5	185.2	185.8	203.0

Fig. 13 shows the effect of k_2 on the results. Overall, $\overline{R_S}$ and $\overline{T_{ED}}$ decrease with the increase of k_1, and the peak of $R_{D,k}$ changes from k=3 to k=2. This is mainly because when the initial interval is large and k_2 is small, the number of $d_{i,i+1}$ belonging to the term "far" increases in the fuzzification process. This leads to the reduction of $V_{I,i}$, the increase of the distance between the current and the front aircraft, and the increase of flight time. As previously mentioned, results are also affected by performance limitations, fuzzy logic rules, and the DFVD algorithm, $\overline{R_S}$ and $\overline{T_{ED}}$ will not increase or decrease indefinitely.

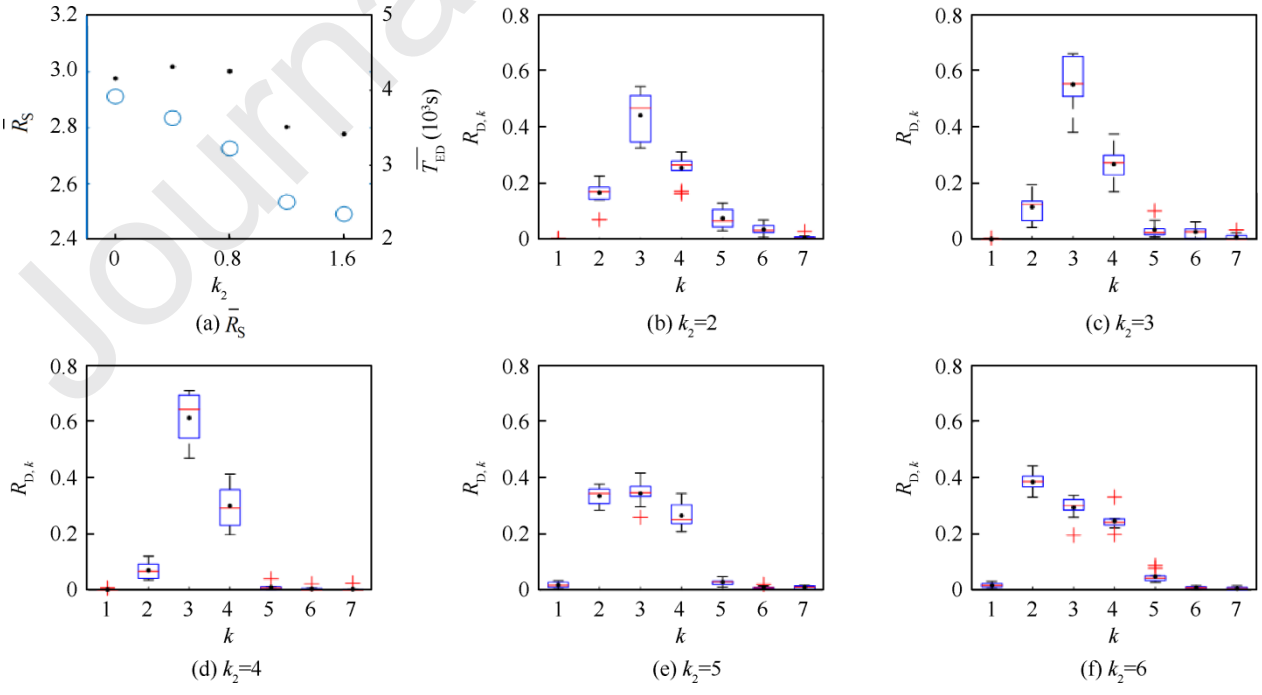

Fig. 13 Results of k_2 impacts on indicators.

Comparing the results of k_1 and k_2 in Table 10 with Figs. 12 and 13, we can see that the trends of $\overline{T_{\mathrm{ED}}}$ and $\overline{V_{\mathrm{I}}}$ are consistent. However, the insignificant changes of $\overline{T_{\mathrm{ED}}}$ are not clearly related to $\overline{V_{\mathrm{I}}}$. The change of $\overline{T_{\mathrm{ED}}}$ is also affected by many other factors such as flight distance and flight altitude.

4.5.3. Impacts of distance membership functions parameters

Based on the baseline experiment, we change the parameters of U_{f} membership (k_3) at first, and then change the parameters of U_{r} membership (the combination of k_4 and k_5). The trend of the vertical profile, flight speed, and R_{S} of each aircraft are similar with Fig. 10. Fig. 14 shows the effect of k_3 on the results.

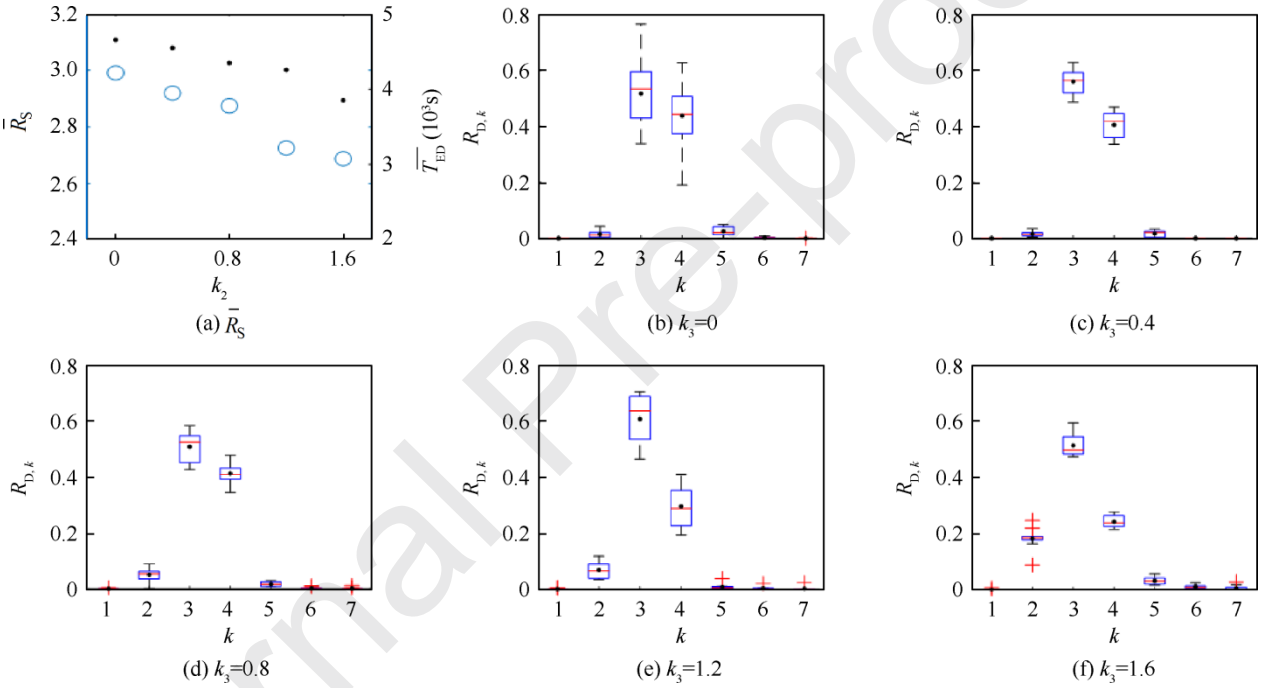

Fig. 14 Results of k_3 impacts on indicators.

As k_3 increases in Fig. 14, $\overline{R_{\mathrm{S}}}$ ("○" in subfigure a) and $\overline{T_{\mathrm{ED}}}$ ("•" in subfigure a) all decrease. This is mainly because the slope of the membership function will increase as k_1 increases. A larger initial interval will make $d_{i-1,i}$ belong to the term "far" more often in the fuzzification process, resulting in acceleration and spacing decrease. From Figs. 14 (b)-(f), we can see that $R_{\mathrm{D},3}$ is always at the peak position in different k_3. The decrease of $R_{\mathrm{D},k}$ ($k\geqslant 4$) and the increase of $R_{\mathrm{D},k}$ ($k\leqslant 2$) cause a decrease as k_3 increases.

Different combinations of [k_4, k_5] have little effect on $R_{\mathrm{D},k}$. Table 11 records the results of $\overline{R_{\mathrm{S}}}$, $\overline{T_{\mathrm{ED}}}$ and $\overline{V_{\mathrm{I}}}$ under 16 combinations of [k_4, k_5]. $\overline{T_{\mathrm{ED}}}$ is small when [k_4, k_5]=[0, 2.5] and [k_4, k_5]=[0.5, 2.5], due to the high average descent speed. The combination of [k_4, k_5] in other cases has little effect on the results.

Table 11 Indicator comparison for distance between adjacent aircraft.

Number	$[k_4, k_5]$	$\overline{R_S}$	$\overline{T_{ED}}$ (s)	$\overline{V_I}$ (kt)
1	[0, 2.5]	2.6391	3640	217.0
2	[0, 3]	2.7533	4157	190.8
3	[0, 3.5]	2.7745	4211	187.8
4	[0, 4]	2.7382	4066	196.2
5	[0.5, 2.5]	2.6609	3871	207.8
6	[0.5, 3]	2.8086	4311	186.9
7	[0.5, 3.5]	2.7138	4100	189.5
8	[0.5, 4]	2.7198	4039	193.4
9	[1, 2.5]	2.7058	4019	198.9
10	[1, 3]	2.7998	4297	187.7
11	[1, 3.5]	2.7092	4140	188.8
12	[1, 4]	2.6708	4055	189.9
13	[1.5, 2.5]	2.7544	4166	190.8
14	[1.5, 3]	2.7256	4255	185.8
15	[1.5, 3.5]	2.6954	4107	188.1
16	[1.5, 4]	2.7466	4108	192.8

4.6. Case study and analysis

In this section, we analyze the impacts of 4 factors on results. These factors are separation standard, aircraft category, initial separation, and initial height. The relevant parameters of the membership functions are set as [k_1, k_2, k_3, k_4, k_5]=[4, 4, 0, 1.5, 3]. Other parameters of the control experiment are the same as Section 4.3.2. Control experiment results are illustrated in Table 12.

Table 12 Indicators for control experiment.

$\overline{R_S}$	$\overline{T_{ED}}$ (s)	$\overline{V_I}$ (kt)	$\overline{R_{D,1}}$	$\overline{R_{D,2}}$	$\overline{R_{D,3}}$	$\overline{R_{D,4}}$	$\overline{R_{D,5}}$	$\overline{R_{D,6}}$	$\overline{R_{D,7}}$
2.9840	4677	174.1	0.0000	0.0143	0.5024	0.4679	0.0152	0.0002	0

4.6.1. Impacts of safety interval criterion

Experiments were carried out using the RECAT criterion in Table 1 to study the effect of the interval criterion on the results, and the results are recorded in Table 13. Comparing it with Table 12, we can see that $\overline{R_S}$, $\overline{V_I}$, and $\overline{R_{D,k}}$ have no significant changes, and the proposed DFVD method can be applied to different interval criteria. But $\overline{T_{ED}}$ in Table 13 is significantly smaller than that in Table 12. This is because the required interval of RECAT is reduced relative to CCAR[45], so the same number of aircraft can fly the same distance in less time.

Table 13 Results of interval criterion impacts on indicators.

$\overline{R_S}$	$\overline{T_{ED}}$ (s)	$\overline{V_I}$ (kt)	$\overline{R_{D,1}}$	$\overline{R_{D,2}}$	$\overline{R_{D,3}}$	$\overline{R_{D,4}}$	$\overline{R_{D,5}}$	$\overline{R_{D,6}}$	$\overline{R_{D,7}}$
2.9500	3888	175.0	0.0000	0.0224	0.5207	0.4364	0.0205	0	0

4.6.2. Impacts of aircraft category

To study the impact of aircraft categories on the results, we carried out two groups of experiments. The first and the second group only involve the H and the M category aircraft (CCAR C criterion in Table 4), respectively. Results are recorded in Table 14. Compared to Table 12, $\overline{R_S}$, $\overline{V_I}$, and $\overline{R_{D,k}}$ have no significant changes. The proposed DFVD methods can well achieve interval management under different combinations of aircraft categories. However, $\overline{T_{ED}}$ is significantly reduced compared to Table 14. This is because of the situation that smaller aircraft flies following the larger aircraft will appear in the mixed operation mode (e.g. A320 flies following A380). In this case, the required flight safety interval would be much greater than the mode of single-category operation. Therefore, the

same number of aircraft take longer to fly the same distance in the mixed operation mode. The DFVD has shorter interval management time in a single category operation mode.

Table 14 Results of aircraft category impacts on indicators.

CCAR category	$\overline{R_S}$	$\overline{T_{ED}}$ (s)	$\overline{V_I}$ (kt)	$\overline{R_{D,1}}$	$\overline{R_{D,2}}$	$\overline{R_{D,3}}$	$\overline{R_{D,4}}$	$\overline{R_{D,5}}$	$\overline{R_{D,6}}$	$\overline{R_{D,7}}$
H	3.0972	3925	174.8	0	0.0060	0.4328	0.5234	0.0347	0.0021	0.0001
M	2.9972	3780	175.9	0	0.0195	0.4827	0.4703	0.0275	0	0

4.6.3. Impacts of initial spacing

We set 10 different initial intervals to analyze its effect. The initial spacing of the front and rear aircraft is generated randomly between $[S_{I,1}, S_{I,2}]\bullet d_{IC}$ shown in Table 15, as well as the result of $\overline{V_I}$. Changes of $\overline{R_S}$, $\overline{T_{ED}}$, and $\overline{R_{D,k}}$ are shown in Fig. 15.

Table 15 Initial spacing and result of $\overline{V_I}$.

Number	$[S_{I,1}, S_{I,2}]\bullet d_{IC}$	$\overline{V_I}$ (kt)
1	[2, 3]	217.0
2	[2, 4]	190.8
3	[2, 5]	187.8
4	[2, 6]	196.2
5	[3, 4]	207.8
6	[3, 5]	186.9

7	[3, 6]	189.5
8	[4, 5]	193.4
9	[4, 6]	198.9
10	[5, 6]	192.8

Combining Table 15 and Fig. 15 (a), we find that $\overline{R_S}$ increases with $S_{I,1}$ and $S_{I,2}$, respectively. From Fig. 15 (b), we can see that $R_{D,2}$ and $R_{D,3}$ decrease while $R_{D,k}\,(k>3)$ increases with the increase of No., which directly leads to the increase of $\overline{R_S}$. An increase in both $S_{I,1}$ and $S_{I,2}$ results in an increase in the average of the initial interval generated randomly, which takes longer to reduce the spacing of the flight sequence to an appropriate interval level. The longer the interval adjustment time in the early stage, the larger the $\overline{R_S}$. The spacing can eventually be controlled at a reasonable level because of the DFVD. $\overline{T_{ED}}$ changes little because $\overline{V_I}$ is not greatly affected by the initial interval, as shown in Table 15.

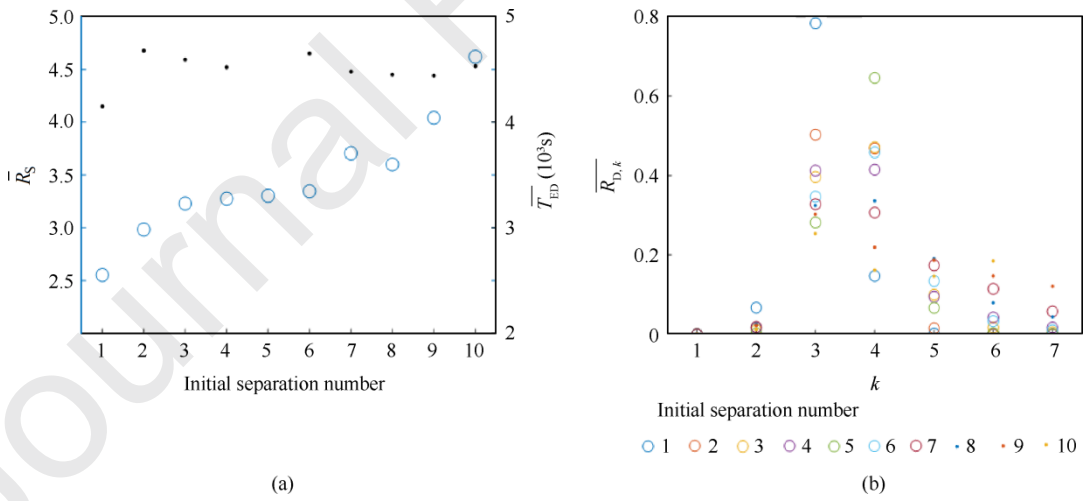

Fig. 15 Results of initial spacing impacts on indicators.

4.6.4. Impacts of the range of initial height

To study the effect of the initial height on the results, H_S changes from 6 km to 8 km with a step of 500 m. Results are shown in Fig. 16. As H_S increases, $\overline{R_S}$ decreases and $\overline{T_{ED}}$ increases, which is safe and efficient in actual operation. As H_S changes from 6 km to 8 km, the results of $\overline{V_I}$ are: 203.2, 189.4, 183.3, 177.3, 174.1 kt,

respectively. The primary reason for these changes is that the entire descending process is a deceleration process. This allows the aircraft sequence to decelerate faster, with reduced spacing. Ultimately aircraft fly at a lower speed with a shorter spacing for the remaining flight range.

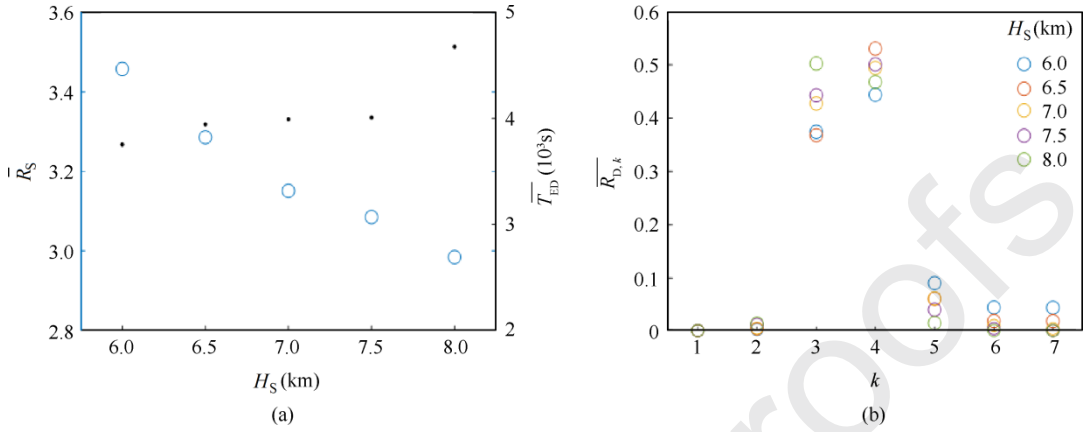

Fig. 16 Results of initial height impacts on indicators.

5. Conclusions

Based on the fuzzy control method, we propose a flight interval management system specifically for the en-route descent stage, which aims to achieve the dynamic autonomous interval management for the aircraft sequence by adjusting their IAS in real time with wind uncertainty. Analysis results are briefly illustrated as follows.

(1) Results of the proposed DFVD method outperform actual statistic data in interval management, reducing aircraft en-route descent time by 29.54%. In addition, the wind uncertainty is well disposed compared to the general method.

(2) The bounds of U_f, U_r, and U_v membership functions, as well as the parameter of U_f, significantly affect the results with high sensitivity. In addition, dynamically generating the bound of U_v membership is safer and more stable than the static generation method.

(3) The proposed DFVD method can adapt to different interval criteria and aircraft categories. Considering the influence of the initial interval and the initial height on the results, if the initial altitude is high, the initial interval can be appropriately increased to improve the performance of DFVD. Not only does this increase the spacing and improve safety, but it also does not affect the total en-route descent time of the flight sequence.

The proposed method, the generated trajectory, and flight parameters provide valuable guidance for realizing autonomous interval management operations in the field of ATM and FIM. However, this research was carried out for the normal flight sequence, and there are many impacts during actual operations. Future research will further consider these disruptions, as well as the fuel consumption and emission issues that arise from them.

References

1. Alexandre DJ. IATA annual review 2020 Amsterdam: IATA[Internet]. [cited 2022 Oct 3]. Available from: https://www.iata.org/contentassets/c81222d96c9a4e0bb4ff6ced0126f0bb/iata-annual-review-2020.pdf.

2. Air passenger numbers to recover in 2024. Amsterdam: IATA[Internet]. [updated 2022 Mar 1; cited 2022 Oct 3]. Available from: https://www.iata.org/en/pressroom/2022-releases/2022-03-01-01/.

3. Eurocontrol. European aviation in 2040 - challenges of growth. Brussels: Eurocontrol [Internet]. 2018 [cited 2022 Oct 3]. Available from: https://www.eurocontrol.int/publication/challenges-growth-2018.

4. National Academies of Sciences, Engineering, and Medicine. *Autonomy research for civil aviation: Toward a new era of flight*. Washington, D.C.: The National Academies Press; 2014. p. 23-4.

5. Socha V, Hanáková L, Valenta V, et al. Workload assessment of air traffic controllers. *Transp Res Procedia* 2020;51: 243–51.

6. Ballin M, Wing D, Hughes M, et al. Airborne separation assurance and traffic management - Research of concepts and technology. Reston: AIAA; 1999. Report No.: AIAA-1999-3989.

7. SESAR Joint Undertaking. European ATM master plan 2020 - executive view Luxembourg: Publications Office of the European Union [Internet]. [cited 2022 Oct 3]. Available from: https://www.sesarju.eu/masterplan2020.

8. Five-year action plan for promoting the construction of new civil aviation infrastructure. Beijing: Air Traffic Management Bureau of Civil Aviation Administration of China; 2020. Report No.: 2020-63 [Chinese].

9. Riedel T. A novel control approach to improve speed commands and pilot workload for flight-deck based interval management. *31st congress of the international council of the aeronautical sciences.* Bonn: ICAS; 2018. p. 1-10.

10. Itoh E, Uejima K. Applying flight-deck interval management based continuous descent operation for arrival air traffic to Tokyo international airport. *10th ATM seminar.* Chicago: FAA/EUROCONTROL; 2013. p. 1-10.

11. Brittain M, Yang XX, Wei P. A deep multi-agent reinforcement learning approach to autonomous separation assurance. arXiv preprint: 2003.08353, 2020.

12. Lascara B, Guensch C, Weitz LA, et al. Leveraging interval management to improve air traffic operations during departure. Reston: AIAA; 2016. Report No.: AIAA-2016-1611.

13. Barmore B, Penhallegon WJ, Weitz LA, et al. Interval management: development and implementation of an airborne spacing concept. Reston: AIAA; 2016. Report No.: AIAA-2016-1608.

14. Campbell SE, Clemons E. Preliminary investigation into the use and coverage of a crowd-sourced airborne weather radar network. Reston: AIAA; 2017. Report No.: AIAA-2017-3594.

15. Sandberg M, Reynolds T, McPartland M, et al. Assessing Wind Impacts on Flight Interval Management Performance. Reston: AIAA; 2013. Report No.: AIAA-2013-4406.

16. Tulder PV. Flight deck interval management flight test final report. Washington, D.C.: Report No.: NASA-CR-2017-219626.

17. Guan XM, Lyu RL, Shi HX, et al. A survey of safety separation management and collision avoidance approaches of civil UAS operating in integration national airspace system. *Chin J Aeronaut* 2020;**33**(11):2851–63.

18. Swieringa KA, Underwood MC, Barmore B, et al. An evaluation of a flight deck interval management algorithm including delayed target trajectories. Atlanta, GA. Reston: AIAA; 2014. Report No.: AIAA-2014-3148.

19. Sun MH, Abraham S, Singh N, et al. Waypoint-based flight-deck interval management. Reston: AIAA; 2020. Report No.: AIAA-2020-2101.

20. Singh N, Abraham S, Sun MH, et al. Optimization of waypoint-based flight-deck interval management for NextGen concept of operations. Reston: AIAA; 2021. Report No.: AIAA-2021-0780.

21. Riedel T, Takahashi M, Itoh E, et al. Pilot-centered evaluation of flight-deck interval management control laws using an A320 simulator. *J Aircr* 2020;**57**(5):974–84.

22. Tang XM, Zheng PC. Aircraft autonomous separation control under sequential flying conditions. *J Nanjing Univ Aeronaut Astronaut* 2019;**51**(6):742–8 [Chinese].

23. Hubbs C, Shay R. Aircraft, airspace, and the use of energy management based algorithms to conduct flight deck interval management (IM). *2017 IEEE/AIAA 36th digital avionics systems conference (DASC)*. Piscataway: IEEE Press; 2017. p. 1–8.

24. Brittain M, Wei P. Autonomous air traffic controller: A deep multi-agent reinforcement learning approach. arXiv preprint: 1905.01303, 2019.

25. Brittain MW, Wei P. Towards autonomous air trac control for sequencing and separation - a deep reinforcement learning approach. Reston: AIAA; 2018. Report No.: AIAA-2018-3664.

26. Brittain MW, Yang XX, Wei P. Autonomous separation assurance with deep multi-agent reinforcement learning. *J Aerosp Inf Syst* 2021;18(12):890–905.

27. Gaydos TL, Weitz LA. Designing stochastic optimal control laws for interval management. Reston: AIAA; 2016. Report No.: AIAA-2016-1853.

28. Weitz LA, Swieringa KA. Comparing interval management control laws for steady-state errors and string stability. Reston: AIAA; 2018. Report No.: AIAA-2018-1340.

29. White AL. An elementary algorithm for autonomous air terminal merging and interval management. Reston: AIAA; 2017. Report No.: AIAA-2017-1322.

30. Brittain M, Wei P. Autonomous separation assurance in an high-density en route sector: a deep multi-agent reinforcement learning approach. *2019 IEEE intelligent transportation systems conference (ITSC)*. Piscataway: IEEE Press; 2019. p. 3256–62.

31. Riedel T, Takahashi M, Itoh E. Optimisation of interval management–speed planning using SMPSO. *Aeronaut J* 2020;**124**(1281):1819–45.

32. Barmore B, Swieringa KA, Underwood M, et al. Development of an interval management algorithm for delayed traffic. Reston: AIAA; 2016. Report No.: AIAA-2016-1851.

33. Arabacioglu BC. Using fuzzy inference system for architectural space analysis. *Appl Soft Comput* 2010;**10**(3):926–37.

34. Jenab K, Pineau J. Automation of air traffic management using fuzzy logic algorithm to integrate unmanned aerial systems into the national airspace. *Int J Electr Comput Eng IJECE* 2018;**8**(5):3169.

35. Cook B, Cohen K, Kivelevitch EH. A fuzzy logic approach for low altitude UAS traffic management (UTM). Reston: AIAA; 2016. Report No.: AIAA-2016-1905.

36. Ntakolia C, Lyridis DV. A n − D ant colony optimization with fuzzy logic for air traffic flow management. *Oper Res* 2022;**22**(5):5035–53.

37. Khan BA, Lai NS. An intelligent traffic controller based on fuzzy logic. *Proceedings of the 1st international conference on green computing, technology and innovation* (ICGCTI'13). Society of Digital Information and Wireless; 2013. p. 89-93.

38. Baridam B. An intelligent air traffic control system using fuzzy logic model. *Int. J. Appl. Inf. Syst* 2018; **11**(12): 1-9.

39. Ören A, Koçyığıt Y. Landing sequencing modelling with fuzzy logic: Opportunistic approach for unmanned aerial systems. 2016 international conference on unmanned aircraft systems (ICUAS). Piscataway: IEEE Press; 2016. p.: 943–8.

40. Volpe Lovato A, Hora Fontes C, Embiruçu M, et al. A fuzzy modeling approach to optimize control and decision making in conflict management in air traffic control. *Comput Ind Eng* 2018;**115**: 167–89.

41. Eurocontrol. User manual for the base of aircraft data (BADA) revision 3.7. Brussels: Eurocontrol; 2009. Report No.: 2009-003.

42. Pérez-Castán JA, Rodríguez-Sanz Á, Pérez Sanz L, et al. Probabilistic strategic conflict-management for 4D trajectories in free-route airspace. *Entropy* 2020;**22**(2):159.

43. Abrous A, Wamkeue R, Berkouk EM. Modeling and simulation of a wind model using a spectral representation method. 2015 3rd International Renewable and Sustainable Energy Conference (IRSEC). Piscataway: IEEE Press; 2016. p.:1–6.

44. Peng ZH, Zhang JF, Xiang T, et al. Benefits derived from arrival management and wake turbulence re-categorization in China. *Transportation Research Record* 2021;**2675**(11):373–83.

45. Wei ZQ, Li XC, Liu F. Research on aircraft wake vortex evolution and wake encounter in upper airspace. *Int J Aeronaut Space Sci* 2022;**23**(2):406–18.

Declaration of interests

☒ The authors declare that they have no known competing financial interests or personal relationships that could have appeared to influence the work reported in this paper.

☐The authors declare the following financial interests/personal relationships which may be considered as potential competing interests:

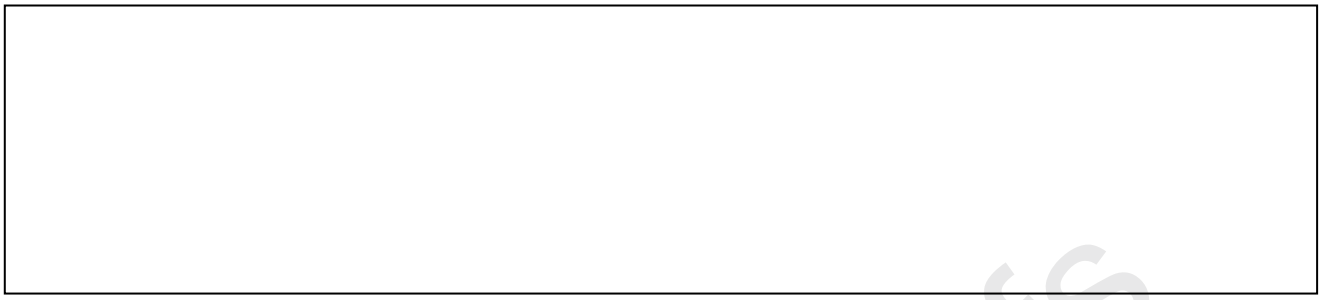

2023-07-13

Automatic interval management for aircraft based on dynamic fuzzy speed control considering uncertainty

Yuan, Jie

Elsevier

Yuan J, Pei Y, Xu Y, et al., (2023) Automatic interval management for aircraft based on dynamic fuzzy speed control considering uncertainty, Chinese Journal of Aeronautics, Available online 13 July 2023

https://doi.org/10.1016/j.cja.2023.07.008